Exploring the Role of Damping in a Passive Prosthetic Knee through Modeling, Design, and Testing

by

Nina T. Petelina

B.S. in Mechanical Engineering
Massachusetts Institute of Technology (2017)

Submitted to the Department of Mechanical Engineering
in partial fulfillment of the requirements for the degree of

Master of Science in Mechanical Engineering

at the

MASSACHUSETTS INSTITUTE OF TECHNOLOGY

September 2019

Author ..... Signature redacted
Department of Mechanical Engineering
August 31st, 2019

Certified by ..... Signature redacted
Amos G. Winter, V
Associate Professor of Mechanical Engineering
Thesis Supervisor

Accepted by ..... Signature redacted
Nicolas Hadjiconstantinou
Professor of Mechanical Engineering
Graduate Officer

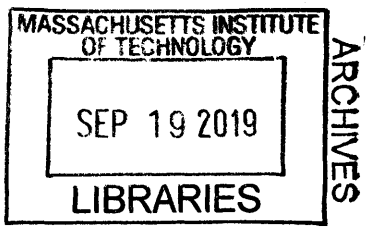

Exploring the Role of Damping in a Passive Prosthetic Knee through Modeling, Design, and Testing

by

Nina T. Petelina

Submitted to the Department of Mechanical Engineering
on August 31st, 2019, in partial fulfillment of the
requirements for the degree of
Master of Science in Mechanical Engineering

Abstract

With about 440,000 people with an above-knee amputation in India alone, there is a great need for high performance prosthetic knee. Due to socio-economic stigma associated with amputation, one of the main requirements for a lower limb prosthesis is achieving able-bodied kinematics. However, the prostheses available in developing countries, such as India, primarily focus the design on stability and low cost.

This study presents a shear-based rotary viscous damper design for late stance and swing flexion for a passive single-axis knee prosthesis. The optimal normalized damping coefficient range of $0.012 - 0.014 \frac{Nm}{kg * \frac{rad}{s}}$ was determined by optimizing a set of passive components to replicate a knee moment for an able-bodied subject and transtibial amputee wearing a fully characterized prosthetic foot. Dampers with a stacked fin architecture, where a highly viscous fluid is sheared between neighboring disks, were built with a range of damping coefficients from 0.37 to 1.80 Nm/(rad/s).

The performance of dampers was evaluated through field and clinical testing with unilateral transfemoral amputees. The results of the studies showed that not only damping is required to prevent hyperflexion, but the optimal damping range allows achieve a peak knee flexion close to able-bodied. In future design, the validated damping selection framework will be used to expand the prosthetic knee design to other gait activities such as walking at different speeds, on slopes or uneven terrains.

Thesis Supervisor: Amos G. Winter, V
Title: Associate Professor of Mechanical Engineering

Acknowledgments

I would like to thank Professor Amos Winter for hiring me to join the prosthetics team, for the support, feedback on my work, as well as his amazing ability of encouraging enthusiasm for the project.

It's very important to note our collaborators from both India and Chicago. I would like to thank the technicians and staff at the BMVSS, specifically, Dr. Pooja Mukul, for their support and contributions on this project. I would also like to thank Dr. Matthew J. Major, Jenny A. Kent, and Rebecca Stine at Northestern University for their help with the knee testing. Most importantly, I would like to thank all of our subjects that found time to participate in our experiments.

I'm very thankful for the GEAR Lab prosthetics team: Murthy, Victor, and Brett, and our adventures in understanding human gait and our constant travelling around the world. Next I would like to thank my GEAR lab and MIT MakerWorkshop family, friends, and roommates that made my first two years in graduate school so fun and exciting.

And of course, I am thankful for my family and Wesley for their endless love, support, and encouragement.

I am also grateful to the following programs for funding this project:

National Science Foundation (Award no. 1653758)

Indo-US Collaborative Program on Affordable Medical Devices (NIH Project no. 1R03HD092676-01)

Tata Center for Technology and Design at MIT

Contents

List of Figures

List of Tables

Chapter 1

Introduction

1.1 Project Background and Motivation

In 2011, a collaboration between the Bhagwan Mahaveer Viklang Sahayata Samiti (BMVSS, a.k.a. "Jaipur Foot" organization) and MIT GEAR Lab was established to develop a prosthetic knee for above-knee amputees in India. BMVSS, a non-governmental organization (NGO) based in Jaipur, India, is the largest organization helping persons with disabilities in the world [1]. Since its opening in 1975, BMVSS has helped over 1.78 million amputation and polio patients and distributes approximately 29,400 lower leg prosthetics every year. Although BMVSS is only funded by donations and government subsidies, all prosthetic limb, assistive devices, and the fittings are available to people free of charge.

Global studies have estimated that there are approximately 25 million lower limb amputees in the world. Based on the "Disabled Persons in India" report by National Sample Survey Organization of India and other reports in the literature [36, 32], Narang [35], estimated that there are 950,000 people with lower limb amputations in India alone and 440,000 of those people have above knee amputations. About three quarters of Indians with amputations live in a rural setting [30]; moreover, studies have shown that many of them are from low income families. Studies have also shown that Indians with amputations tend to suffer social-economical stigmas due to their disability[25, 43, 48]. These results were supported by a survey from

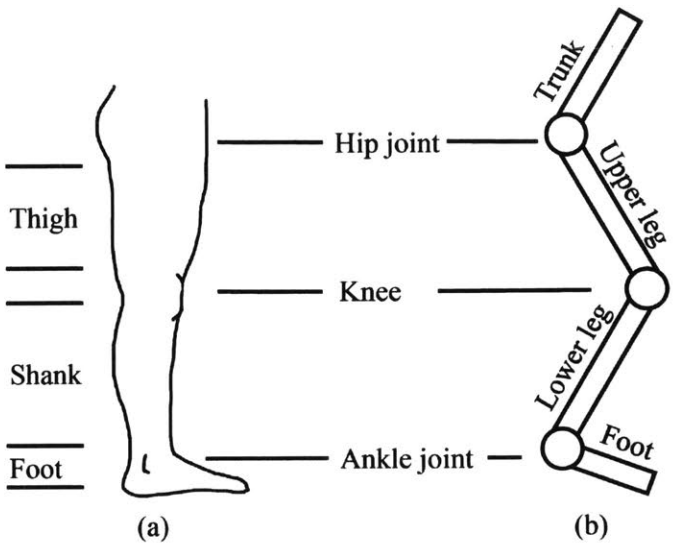

Figure 1-1: (a) Nomenclature for human leg segments and (b) a two-dimensional segment model used for gait analysis.

Narang [35], who interviewed 19 subjects at BMVSS. His study showed that the main cause of amputation was trauma (74%), most amputees lived in a village (76%), and approximately half (46%) of the subjects became unemployed after their amputation.

Based on these results, BMVSS and MIT identified the following main design requirements for a high-performance, low-cost prosthetic knee [35]:

- Allows able-bodied gait on flat ground
- Provides stability on uneven terrain
- Costs less than $100 to manufacture

1.2 Biomechanics of Human Gait

The human leg can be divided into six segments: foot, ankle, shank (leg or the lower leg), knee, thigh or the upper leg, and hip (Fig.1-1). Anatomical motion is usually described in three planes: sagittal (viewing a person from the side), frontal (viewing a person from the front), and transverse (viewing a person from above). Most of this thesis will analyze motions in the sagittal plane, unless specified otherwise.

The gait cycle is a periodic motion that allows people to support and propel themselves. Although this thesis will refer only to the over-ground walking gait cycle, the term gait cycle can also refer to running, hopping, etc. A complete gait cycle covers one full sequence of motion for the right or left leg between consecutive heel strikes. The gait cycle (or stride) is divided into two main phases:"stance" when the foot is on the ground, and "swing" when the foot is off the ground. The stance phase begins when the heel of the specified leg makes contact with the ground (heel strike) and ends when the toe of the foot loses contact with the ground (toe-off). In this thesis, the gait cycle is normalized by time and is presented as percentage of the stride. It is important to note that the stance and swing phases make up approximately 60% and 40% of the gait cycle, respectively (Fig. 1-3). Stance phase is further divided into the single limb support phase where only one leg is on the ground and the double limb support phase where both legs are on the ground.

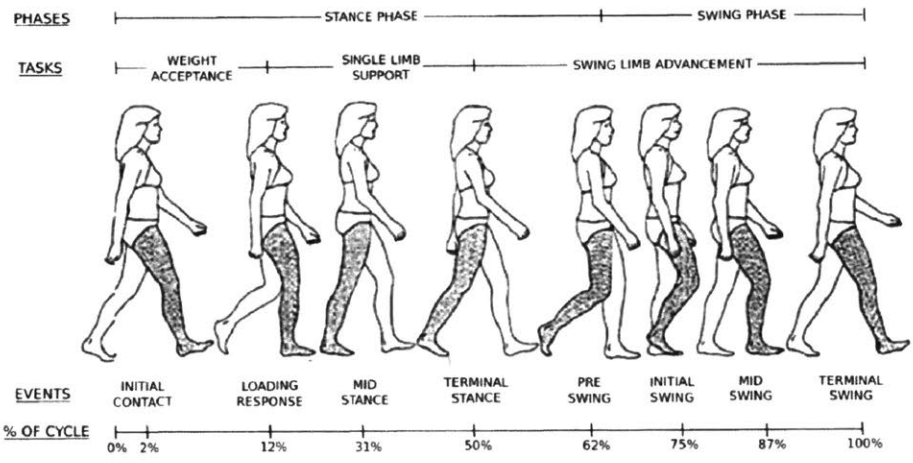

Figure 1-2: Typical phases of an able-bodied human gait cycle. Adapted from [42]

Another way of dividing the gait cycle is based on the forward progression of the body. The Rancho Los Amigo Gait Analysis Committee proposed a taxonomy that is commonly used in literature [12]. The phases are: initial contact, loading response, mid-stance, terminal stance, pre-swing, initial swing, mid-swing, and terminal swing (Fig.1-2).

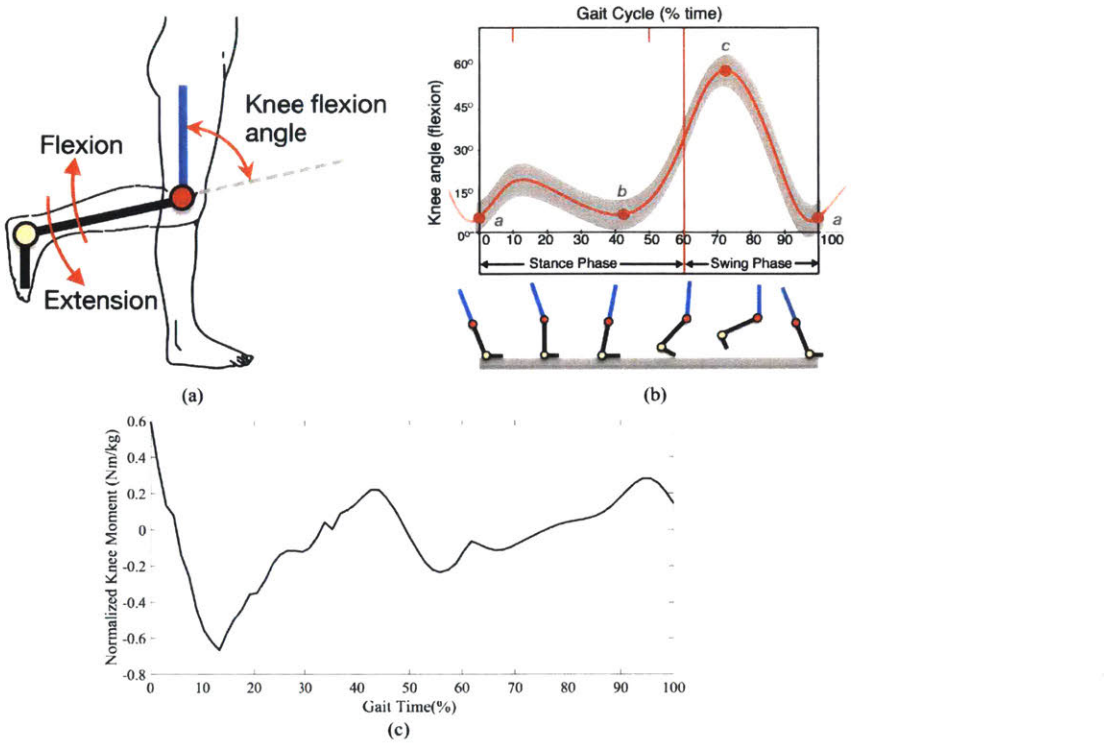

Figure 1-3: (a) Definition of knee flexion and extension convention. The knee flexion angle is the relative angle between the upper and lower leg segments. (b) An example of knee flexion angle throughout a gait cycle, which is divided into stance and swing phases. The red curve shows normative able-bodied kinematics with the standard deviation presented with a grey band. Adapted from [15] (c) An example of normalized knee moment throughout a gait cycle for an able-bodied subject. Adapted from [46]

Human gait is commonly analyzed by measuring kinematics (motion), kinetics (forces and moments), and/or energetics (power and energy). The kinematics of human motion is usually collected by placing markers on the body of the subject and tracking their motion with a high speed camera or with inertial measurement units (IMUs) that collect data using accelerometers and gyroscopes. The kinetic forces are commonly measured using force plates that measure the forces between the foot and the ground (ground reaction force, or GRF). Afterward, the collected kinematic and kinetic data are used to compute the joint forces using inverse dynamics. For inverse dynamics in the sagittal plane, the foot, lower leg, and upper leg are commonly modeled as rigid segments connected with pin joints. The center of mass, radius of gyration, and mass of the segments are estimated using anthropometric data from the literature. In this thesis, the inertial parameters will be computed using regression

equations developed by De Leva [20] unless otherwise specified.

For this thesis, it is important to note the convention that is used for the knee flexion and extension. Angular displacement in the positive direction about the knee joint is considered to be "flexion", and the angular displacement in the negative direction is considered to be "extension". An example of a measured knee angle and moment about the knee joint normalized by weight adapted from Winter [46] is show in Fig. 1-3.

1.3 Prosthesis Terminology and Existing Prosthetic Knee Joints

Lower limb prostheses are often divided into two categories distinguished by the level of the user's amputation: below-knee (transtibial) and above-knee (transfemoral). The terminology presented below mostly applies for both categories. An above-knee prosthesis usually consists of five main components: the foot prosthesis, shank (pylon), knee joint prosthesis, the socket (interface between the prosthesis and the residual limb), and sometimes a suspension belt (Fig. 1-4). The suspension belt may not be required for vacuum sockets that use pressure in order to stay securely on the residual limb. For optimal performance and comfort, each amputee requires a custom made socket and proper prosthetic alignment, where the components are carefully positioned and oriented to allow comfortable standing and walking.

Unfortunately, reduced muscle function from muscle loss and atrophy results in a significant difference between typical transfemoral gait and able-bodied gait. Other factors such as additional and undesirable degrees of freedom of the prosthesis and pain caused by the socket can alter the gait of an amputee. Common compensating gait alterations are lateral trunk bending, abduction (wide walking base), circumduction (semicircle leg motion during swing in the transverse plane), vaulting (standing on the toe on the sound side during swing), swing-phase whips where the heel swings away from the long axis of the body, uneven heel rise, terminal impact right before

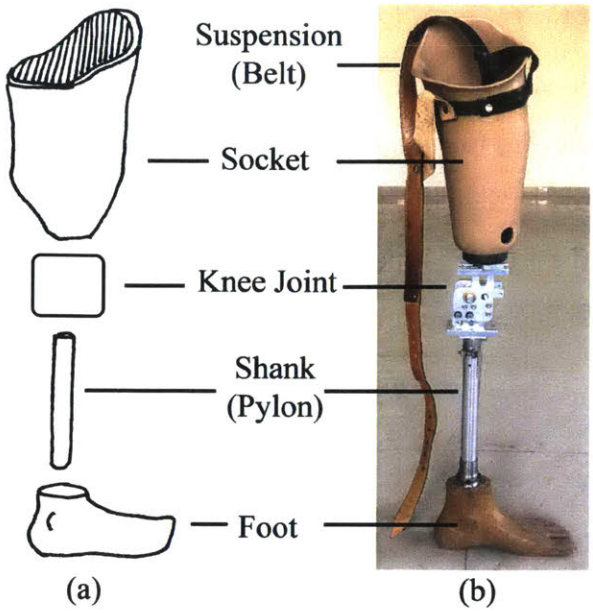

Figure 1-4: (a)schematic and (b) photograph of a typical main components of an above-knee prosthesis: foot, shank (pylon), knee joint, socket and a belt for suspension.

heel strike, and uneven step length and timing [47]. It is important to note that transfemoral amputees have a shorter flexion phase during swing: specifically, knee flexion during terminal stance starts at 60% of the gait cycle instead of 40% [26]. Additionally, unlike transtibial amputees and able-bodied persons, transfemoral amputees tend to prefer to walk with a significantly slower walking speed.

Many different types of knee prostheses have been designed, however, the prosthesis available for the developing world can be generally divided into three main categories: manual locking knees, single-axis knees (free-swinging and braking), and polycentric knees [13]. Currently, there are three types of knee prostheses available at BMVSS: a single-axis manual locking knee joint (Fig. 1-5 (b)), single-axis swinging knee (Fig. 1-5 (c)), and a four-bar knee (Fig. 1-5 (d)).

The exoskeletal knee is kept locked and extended during walking and can be unlocked and bent for sitting. This type of a knee prosthesis is stable during walking and is generally prescribed to new or elderly prosthesis users [41]; however, it does not allow a gait close to able-bodied. Specifically, the exoskeletal (located on the exterior of the prosthesis) knee does not allow knee flexion during stance phase, which provides

shock absorption during loading phase [39], and it also does not allow knee flexion during late stance and swing phases, which provides clearance for the foot during swing. The manufacturing cost of a manual locking knee is approximately $10.

The single-axis free swinging knee does not lock the prosthetic knee, and instead friction within the joint prevents the knee from flexion, and a band prevents hyper-flexion of the prosthetic knee. Similarly to a manual locked knee, it doesn't provide flexion during stance, however it can instead buckle during stance, which can result in a fall of the prosthesis user. An example of both a manual locked and free-swinging knee is the International Committee of the Red Cross (ICRC) endoskeletal (located along the centerline of the prosthesis) prosthetic knee, where the configuration is determined by the lock (Fig. 1-5 (a)).

Another single axis design is the LCKnee designed by Andrysek [14] (Fig. 1-5 (e)). This prosthetic knee uses an automatic lock that keeps the prosthetic knee locked during stance, and unlocks during late stance, allowing the knee to flex during swing phase. The cost of the LCKnee is approximately $50-100.

The four bar knee prosthesis, such as the Stanford-Jaipur knee (Fig. 1-5 (d)) [3], similarly prevents knee flexion during stance phase loading; however, it does allow clearance during swing phase albeit without any motion control. The motion of the knee is characterized by a center of rotation, generally placed behind the knee during stance, which changes with the angles of the bars. This type of prosthesis is usually prescribed to younger, more experienced and active users [41]. The manufacturing cost of a Stanford-Jaipur knee is about $20.

On the other hand, there are two main categories of knee prosthesis in the developed world: "passive knees" (do not contain any external energy source), and "active knee" (which are battery operated). Similarly to the developing world technologies, there are both single and multiple axis of passive prosthetic knees in mature markets, however, they tend to have expensive components, such as hydraulic dampers for knee flexion in both stance and swing phases. These prosthesis are cadence-dependent, which allows the users to walk comfortably at multiple speeds. Active knees tend to use similar components as the passive prosthetic knees; however, they

Figure 1-5: Photographs of different prostheses available in the developing world. All of the examples are passive prostheses, and the figure displays both fully extended and fully flexed configurations. Adapted from [35, 16]

also incorporate sensors that collect kinematic and kinetic data to control the performance of the prosthetic knee. The prosthesis costs for the developed world could range from $2,000 to $75,000 [16], depending on the components used.

1.4 Thesis Outline

This thesis builds upon earlier work done by Narang, Arelekatti, and Winter [35, 16, 34, 33, 31, 19] and primarily focuses on an overview of the prosthetic leg design and a new damper mechanism and its role in the current prosthetic knee design, design framework, and results from experimental studies regarding its performance. The work on the modeling and testing of the prosthetic knee design presented in this thesis were done in collaboration with V.N. Murthy Arelekatti [17].

- **Chapter 2**: An overview of the design framework and the current design of the prosthetic knee are presented, with a focus on the knee components selection, value prediction, and design. This chapter also introduces the U-spring foot prosthesis design used for the modeling and experiments of the prosthetic knee.

- **Chapter 3**: This chapter provides a detailed description of the damper modeling and design process, given prior art review. Additionally, this chapter describes the design of the damper characterization setup.

- **Chapter 4** This chapter presents the results and limitations from numerous testing protocols for the prosthetic leg, including benchtop damper characterization, a qualitative field study in India with BMVSS patients, a quantitative kinematic study with human subjects walking on a treadmill with the prosthesis, and a quantitative kinematic and kinetic study of normal over-ground walking with the prosthesis.

- **Chapter 5** This chapter also discusses the research contributions and recommendations for future design improvements.

Chapter 2

Leg Design

2.1 Prosthetic Foot

The prosthetic foot currently used in BMVSS is the well-known Jaipur foot (Fig. 2-1). The foot was developed in 1968 by Dr. P.K. Sethi to satisfy the specific needs of amputees in India. Although the Jaipur Foot is currently handmade from a block of wood and two rubber blocks with a vulcanized rubber cover, it mimics the appearance of a biological foot, suits the country lifestyle, and is overall a robust and relatively high performance prosthetic foot [18]. A collaboration between BMVSS and Professor Amos Winter at the GEAR Lab was established in 2011 in order to design an affordable, mass-manufacturable prosthetic foot that performs as well as, if not better than, the Jaipur Foot. Similar to the prosthetic knee design, the goal of the project is to design a passive prosthetic foot that replicates able-bodied gait and loading on the foot using affordable materials.

2.1.1 Lower Leg Tragectory Error Framework

As a result of the collaboration, a novel framework, based on a new optimization metric called the Lower Leg Trajectory Error (LLTE), was created by Olesnavage and Winter [38, 37]. The framework maps the mechanical design of a prosthetic foot to its biomechanical performance. In order to design a prosthetic foot that promotes

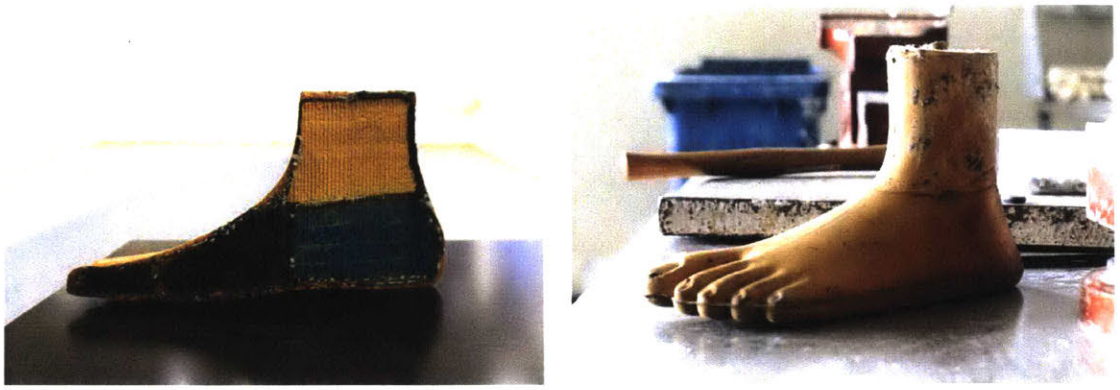

(a) (b)

Figure 2-1: Photographs of the Jaipur Foot. (a) The cross-section of the Jaipur foot showing the wood block, two rubber blocks, and the vulcanized rubber cover. (b) The Jaipur foot has an appearance that mimics a biological foot. Adapted from [44].

a desired shank trajectory during stance, the framework applies reference GRFs and COP data to a constitutive model of the prosthetic foot design to predict how the foot will deform under the expected loading conditions. This deformation determines the trajectory of the lower leg in the sagittal plane, which can be described by three variables: x_{knee}, y_{knee}, and θ. Then, the LLTE is calculated from the normalized root mean square error between this predicted the lower leg trajectory versus the desired target trajectory [37]. The LLTE is calculated for set of discrete points taken at different time intervals during stance. The governing formula for LLTE with N time intervals is:

$$LLTE = \sqrt{\frac{1}{N}\sum_{n=1}^{N}\left[\left(\frac{x_n^{knee} - \hat{x}_n^{knee}}{\bar{x}_{knee}}\right)^2 + \left(\frac{y_n^{knee} - \hat{y}_n^{knee}}{\bar{y}_{knee}}\right)^2 + \left(\frac{\theta_n^{LL} - \hat{\theta}_n^{LL}}{\bar{\theta}_{LL}}\right)^2\right]} \quad (2.1)$$

In the framework, a lower LLTE value corresponds to a prosthetic foot that better replicates the target lower leg trajectory under the expected loading conditions. Therefore, a LLTE value of zero, indicates the foot perfectly produces the desired shank motion.

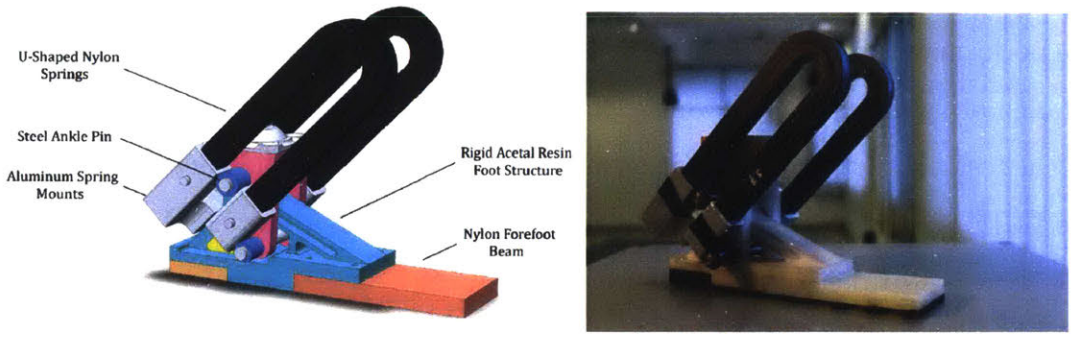

Figure 2-2: The U-spring foot solid model and photograph. The foot prototypes were designed using a LLTE framework in order to achieve able-bodied kinematics. The stiffness of the foot prototype was controlled with U-shaped Nylon springs at the ankle and the forefoot stiffness was controlled with a Nylon beam. Adapted from [44]

2.1.2 U-Spring Foot Design and Testing

In order to validate the LLTE framework, a passive prosthetic foot prototype optimized for replicating able-bodied gait was created using the LLTE method (Fig. 2-2). The foot prototype will be referred in this thesis as the U-spring foot due to the U-shaped springs at the ankle. The U-spring foot is a passive device with two main compliant elements: a beam and U-shaped springs. The springs and the compliant beam are made out of Nylon, and most of structure parts are made out of Acetal resin. The prototype is capable of replicating the quasi-stiffness and range of motion of a physiological ankle during walking, and different U-shaped springs of varying size can be interchanged within the design, providing a range of stiffness from 1.5 to 24 Nm/deg and range of motion of up to 30 degrees.

The foot prototype was evaluated by collecting both kinematic and kinetic data in a motion tracking laboratory with a transtibial subject. The subject walked on a flat ground at a comfortable speed under different U-spring stiffness conditions ranging from 1.5 to 24 Nm/deg. The performance of the prosthetic foot and the springs was evaluated by measuring the center of pressure progression, orientation of the shank, knee joint location, and the ground reaction forces. The results of the study have shown that LLTE was sufficient for predicting a stiffness for the ankle

that allowed close to able-bodied kinematics. However, the study also showed that the performance of the prosthetic feet is not sensitive to an optimal LLTE value; thus, a range of values close to lowest LLTE value show similar performance [37, 38]. The initial testing and characterization of these feet validated the constitutive model of the LLTE and suggested that prosthetic feet designed with lower LLTE values could offer benefits to the user [40, 44].

2.1.3 Influence on the Prosthetic Knee Design

For the testing of the knee prosthesis, the foot selection is crucial, as the behavior of the foot prosthesis will directly influence the performance of the prosthetic knee and its ability to replicate able-bodied kinematics. Although the target knee moments were previously calculated using able-bodied gait data, persons with above knee amputations wearing passive prostheses would not be able to replicate certain features of able-bodied gait, such as power generation at the ankle joint. Persons with below knee amputations wearing passive prostheses also cannot replicate these features of able-bodied gait; therefore, in this study we assumed that gait data from persons with below knee amputations would provide a better target gait of people with above knee amputations than able-bodied gait. Since the U-spring foot is a fully characterized foot that was designed and optimized for below-knee amputees to achieve kinematics closest to able-bodied kinematics, it was chosen as both the target kinematic performance and as the prosthetic foot for clinical studies.

2.2 Knee Design

The knee design presented in this section is based on the previous work by Narang, Arelekatti, and Winter [34, 33, 19, 31]. The overall design requirements are based on the user needs identified by the survey of Narang[35].

- Allows able-bodied gait on flat ground
- Provides stability on uneven terrain

- Costs less than $100 to manufacture

Although these requirements are quite broad, they allowed us to set up a framework for the design of the prosthetic knee presented in previous studies from this project. The low-cost requirement and the environment in which users live dictated that the components of the prosthetic knee had to be passive. The able-bodied kinematics requirement determined the framework for selecting these passive components. Lastly, the stability requirement influenced the engagement pattern of the passive components.

This section presents an overview of the modeling framework for mechanical component selection and introduces the overall design of the prosthetic knee, its components, and their function.

2.2.1 Component Selection

As described above, the component selection was driven by the goal to achieve able-bodied kinematics. In able-bodied gait, the knee motion is controlled by muscles, tendons, and ligaments, however, in the case of a transfemoral amputee, these muscles and tendons are not available. Therefore, in order to achieve able-bodied kinematics, the components in the prosthetic knee have to be tuned to replicate the musculotendon function. In order to optimize the performance of the components, Narang [34, 35] have chosen to replicate the moment about the knee joint as the framework for the component selection. Therefore, this project assumed that by achieving this target knee moment, an amputee will exhibit able bodied kinematics about the knee.

In order to select and optimize the components for the prosthetic knee, target knee moment and kinematics were based on the testing of a fully characterized foot prosthesis, described in the previous section. In previous work, Narang [35] used able-bodied kinematics and kinetics as the target; however, persons with above knee amputations wearing passive prostheses would not be able to replicate certain features of able-bodied gait, such as power generation at the ankle joint. Therefore, in this study, transtibial gait is used as a target because transtibial subjects already provide

the dynamic solution for how to achieve close to able-bodied kinematics using passive feet.

Inertial parameters of the leg segments, such as weight and moment of inertia, can be different for transtibial and transfemoral amputees, and this discrepancy might have an effect on the knee moment. Therefore, the prosthetic knee target moment required for a transfemoral amputee to achieve able-bodied kinematics during normal level-ground walking has to be adjusted. This assumption was based on the studies by Narang [33]. The present study has expanded the inertial parameter theory to account for the changes in mass, center of mass, and radius of gyration. The mass changes are used to calculate the adjusted ground reaction forces (Eqn. 2.2) and the new GRFs are used along with adjusted center of mass and radius of gyration for inverse dynamics calculations.

$$\overrightarrow{GRF}_{pr} = \overrightarrow{GRF}_{ref} - \begin{pmatrix} (m_{ul_{ref}} - m_{ul_{ref}})(\ddot{\overrightarrow{r}}_{ul_{COM}} + g\hat{y}) + \\ (m_{ll_{ref}} - m_{ll_{ref}})(\ddot{\overrightarrow{r}}_{ll_{COM}} + g\hat{y}) + \\ (m_{f_{ref}} - m_{f_{ref}})(\ddot{\overrightarrow{r}}_{f_{COM}} + g\hat{y}) \end{pmatrix} \tag{2.2}$$

The inertial parameters such as mass, center of mass, and moment of inertial of all leg segments were estimated using direct measurements for the prosthetic parts and using coefficients available from literature measurements for physiological leg segments [20, 5]. The foot and shank masses were directly estimated using scales and Solidworks. The residual limb and sound limb segment inertial parameters were estimated using mass coefficients that relate the overall body parameters to segment parameters (Fig. 2-3). Additionally, since the thigh center of mass is not located at the length center of the thigh, a simple correlation was used for a more precise mass estimation. The moment of inertia for the residual limb was calculated by approximating the residual limb as a solid cylinder. The formulas for the mass estimation of the residual limb is presented below:

$$\begin{aligned} M_{residual} &= \frac{L_{residual}}{L_{COM}} * \frac{M_{leg\ segment}}{2}, if\ L_{residual} < L_{COM} \\ M_{residual} &= \left(1 + \frac{L_{residual}}{L_{leg\ segment} - L_{COM}}\right) * \frac{M_{leg\ segment}}{2}, if\ L_{residual} > L_{COM} \end{aligned} \tag{2.3}$$

where $M_{residual}$ is the mass of the residual limb, $L_{residual}$ is the length of the residual limb, $M_{leg\,segment}$ is the approximate mass of the leg segment using coefficients from literature [20], $L_{leg\,segment}$ is the length of a leg segment, L_{COM} is proximal distance to the center of mass of a leg segment.

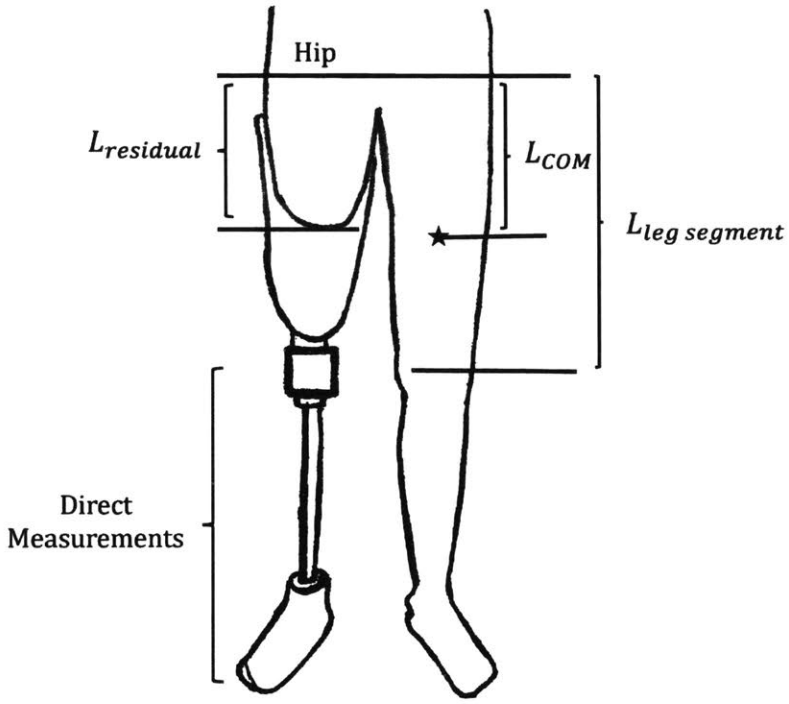

Figure 2-3: Inertial parameters estimation for persons with amputation used either direct measurements for the prosthetic components or scaling coefficients available in literature.

The resulting target knee moment is now ready for component selection. The component selection framework was based on the previous studies of Narang [35, 34]. In order to validate that passive components that would theoretically be effective to replicate an able-bodied gait, the net knee work for a gait cycle was calculated. The net knee work over the gait cycle for both configurations, able-bodied and trans-femoral subjects, was negative. This finding shows that energy is mostly dissipated by the knee, and therefore, passive components can theoretically replicate the knee moment and kinematics.

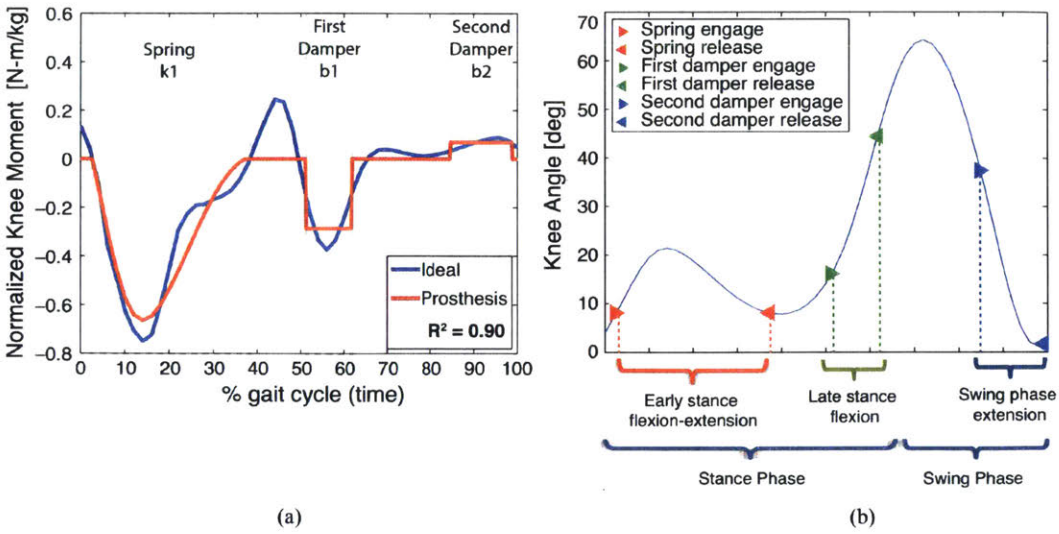

Figure 2-4: Determination of optimal mechanical component coefficients and their engagement computed by Narang. Using inverse dynamics, a spring stiffness ($k1 = 2.9Nm/(kgrad)$) and frictional damping ($b1 = 0.29Nm/kg$ and $b2 = 0.069Nm/kg$) were selected for optimal able-bodied moment replication with $R^2 = 0.90$. (b) The engagement-disengagement points during the gait cycles for the optimal components.

An optimization algorithm was set up in order to determine what combination of passive components, such as clutches, springs, and dampers, would exhibit the best knee moment replication. The algorithm optimized the values based on a cost function represented by the least-squares error between the target moment and the model of passive components. The resulting ideal knee moment replication is presented in Fig. 2-4. The optimization process chose a combination of a linear spring and two constant-force dampers that were engaged independently during three phases of the gait cycle: linear spring during early stance flexion, one damper during swing flexion, and the other damper during swing extension.

Although the component selection allowed close replication of the knee moment, it was not achievable in the design due to the complexity of component engagement. For example, the dampers are only engaged for a part of the flexion or extension phases, which is hard to achieve without using separate clutches for each component. Therefore, a more realistic component selection was chosen based on early design prototypes. In the updated model, the phases of engagement are defined by flexion about the knee axis. Phase 1 starts at heel strike and continues until maximum knee

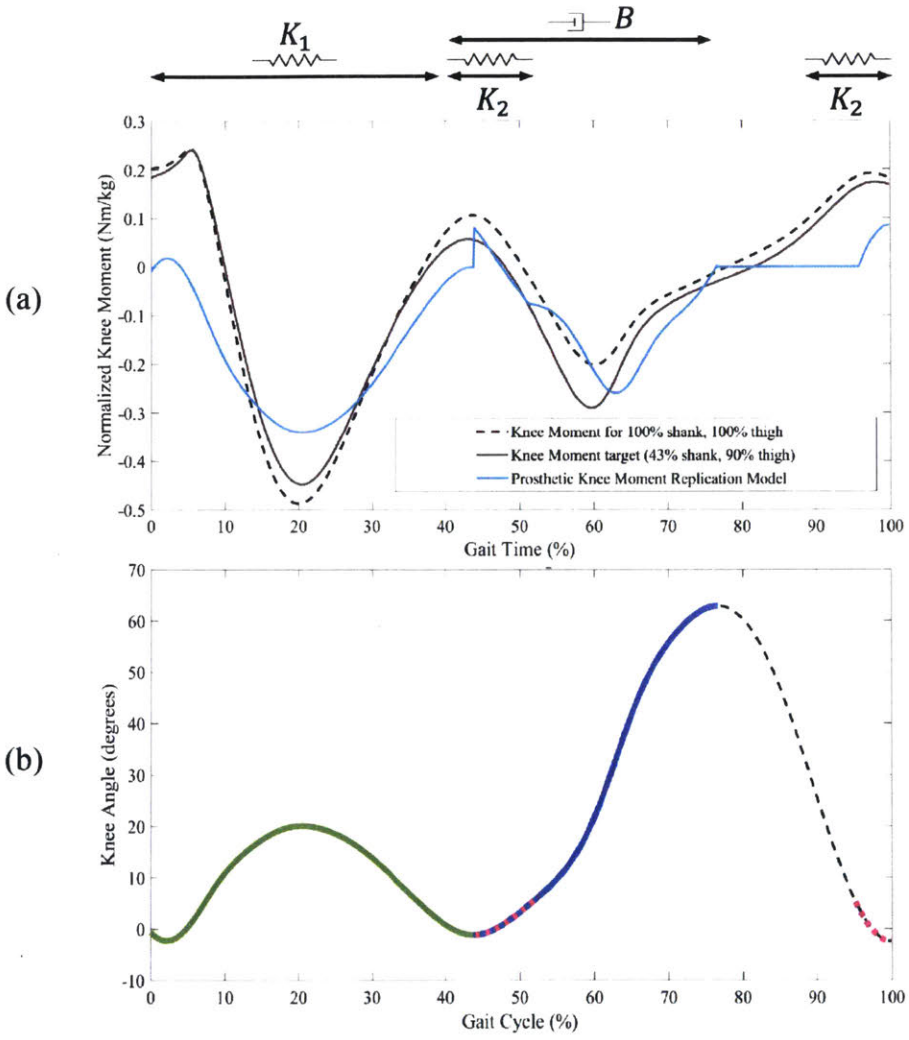

Figure 2-5: (a) Target knee moment for replication was computed by inverse dynamics and taking into account the changes in inertial parameters (in this case 100% foot mass, 43% shank mass, 90% thigh mass). A best-fit analysis estimated that in order to replicate the target knee moment, two springs ($K1 = 0.87Nm/rad$ marked with green line and $K2 = 0.015Nm/rad$ marked with purle dashed line) and one viscous damper ($B = 0.046Nm/(kg * rad/s)$ marked with blue line) is required, with $R^2 = 0.72$. (b) The engagement-disengagement points during the gait cycles for the optimal components.

extension just before terminal stance, Phase 2 starts right after Phase 1 and ends at maximum knee flexion during swing. Phase 3 is the knee extension phase until just before heel strike. The component selection for this engagement pattern was two springs and one damper, and allowed knee moment replication with R^2=0.72 (Fig.2-5). The first spring provides knee flexion during stance phase. The second spring stores energy and acts as a dissipation unit during late swing extension and returns the energy right as Phase 2 starts. Lastly, the damper acts as an energy dissipater and prosthetic knee decelerator.

2.2.2 Knee Mechanical Design

The knee prosthesis design (Fig. 2-6) is based on the previous work by Arelekatti and Winter [16, 31, 19]. The design has a modular structure, which allows for independent changes in the component values or even the complete removal of a component. This modular structure enables the components to be tested, validated, and optimized separately.

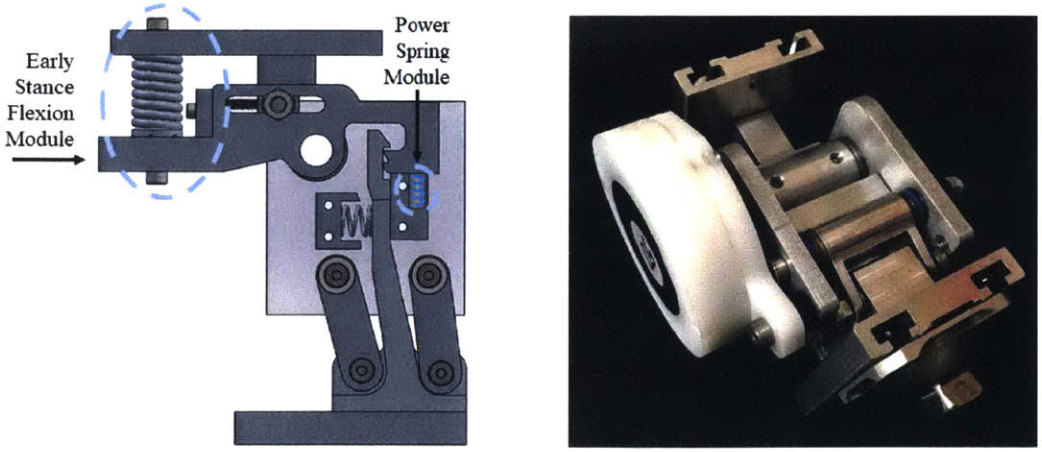

Figure 2-6: (a) Solid model cross-section of the prosthetic knee prototype shows the locking, early stance flexion, and power spring modules. (b) Photograph of the knee prototype with a rotary viscous damper.

The knee design includes four main modules: locking mechanism, early stance flexion module, power spring module, and damping module. The design of the mod-

ules was based on the component selection process described in the previous section. The locking mechanism provides stability during stance phase and allows a smooth transition between stance and swing phases. Moreover, it separates the engagement of the early stance module, responsible for knee flexion during stance, from the power spring and damping. The power spring module accelerates knee flexion just after the latch disengages for swing phase and decelerates knee extension before the next heel strike. Lastly, the damping module decelerates the shank during swing phase, and therefore, controls knee flexion.

Overall, the knee design can be divided into three main components: the knee piece that is connected to the upper leg (the socket), the latch that is connected to the lower leg (the pylon), and the knee body that connects the latch and the knee piece.

Latch

In a gait cycle, the knee exhibits flexion during both stance and swing phases. During stance, knee flexion provides shock absorption from heel strike and leg loading. The knee stays stable and smooths the transition from stance to swing, even though it flexes up to 20 degrees. During swing, knee flexion provides clearance for the foot as it advances to the next step. Therefore, the prosthetic leg must provide stability during stance phase and instability during swing phase. Specifically, the stability of the prosthesis during stance phase provides safety by preventing buckling of the leg, which may lead to falls and injury [41]. Instability during swing allows the prosthetic knee to flex, providing enough clearance to prevent tripping from stubbing the toe on the ground as well as a more able-bodied looking gait. The design of the locking mechanism module directly controls the transition from stability to instability, and can also be used to influence the engagement pattern of the other components of the prosthetic knee design. The following design parameters were identified for the locking mechanism:

- Stability during stance, instability during swing, and smooth transition between the phases

- The robust, safe, and intuitive for use with humans (intuitive and resists a knee moment)

- Does not allow any hyperextension

Various stability solutions have been used for single and multiple axis prosthetic knees in the developing world. Single axis prosthetic knees, such as the exoskeleton prosthetic knee that is currently used at BMVSS, address instability during stance with a manual lock. The user of the prosthesis would lock the knee while walking to prevent any knee flexion and unlock the knee for sitting. This solution results in a gait that is visibly different from able-bodied gait, because the leg is fully extended throughout the entire gait cycle. Multiple axis (or polycentric) prosthetic knees allow knee flexion during swing and provide stability during stance phase, however, they are too stable during terminal stance phase, which delays the transition between stance and swing. An innovative solution for stability in single axis knees was introduced by Andrysek for the LCKnee [14]. The design employs an automatic locking mechanism that locks the knee during stance phase and unlocks it before the start of the swing phase. The lock motion is controlled by the moment exerted by the GRF about the locking mechanism's axis, so that during the gait cycle a flexion moment keeps the knee locked, and an extension moment during pre-swing unlocks the knee. The prosthetic knee design presented in this section employs a similar locking mechanism but with a rear-locking latch that implements a virtual locking axis, which affords flexibility. This improvement also permitted the reduction in the size of the knee prosthesis.

As a person walks, the COP on the foot progresses from heel to toe. Depending on the location of the COP, the GRF causes either an extension or flexion moment about the knee axis. Similarly, based on the location of the latch's locking axis, the combination of a GRF's direction and COP will either keep the lock engaged or disengage it. By varying the position of the locking axis with respect to the knee axis, a zone can be created where specific GRF directions and COP locations both create a flexion moment about the knee and an unlocking moment about the latch.

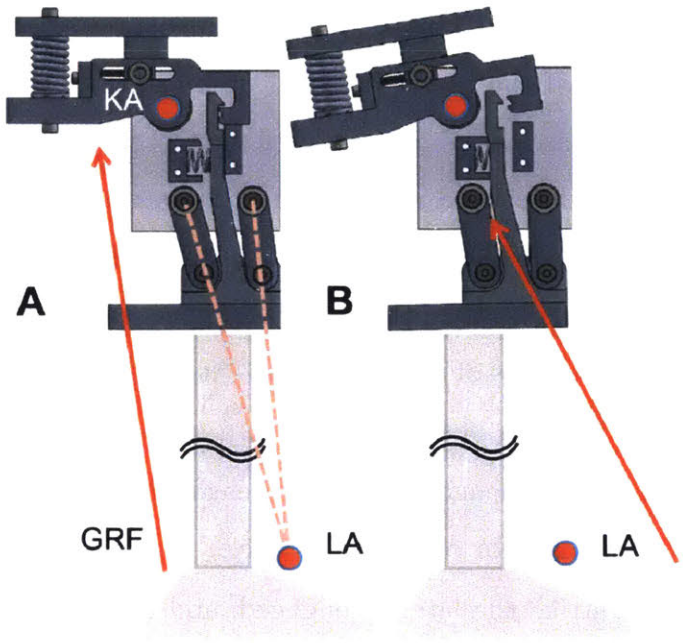

Figure 2-7: The locked (A) and unlocked (B) positions of the stance stability module. The red line represents the ground reaction force and the red dots are the knee axis and the virtual locking axis (KA and LA respectively).

Therefore, creating an instability zone after a specific GRF transition point when the knee is able to flex. In order to replicate able-bodied gait and also fit the engagement pattern presented before, the instability zone was chosen during terminal stance. The locking axis was then chosen to be on the line connecting the knee axis and the GRF transition point.

An additional requirement for the locking axis was to prevent hyperextension, which can cause a user to experience a small wobble during stance when the latch starts to disengage. Therefore, a virtual axis was used for the locking axis. This implementation afforded a more flexible location of the locking axis to achieve a more compact design with desirable hyperflexion of 1 degree.

The resulting knee design was influenced by the locking mechanism, which was integrated into main prosthetic knee components. The knee piece assembly consists of the early stance module that is discussed in more detail in the next section and the locking "hook" for the latch. The "hook" of the knee piece has an additional step that allows the latch to lock at 10 degrees of knee flexion in case the knee doesn't

fully extend before heel strike. This safety mechanism stabilizes the knee and may prevent a fall, especially if the user is walking up an inclined surface. The body of the prosthesis includes hard stops for the latch that prevent hyperextension, a bias spring that preloads the latch and returns it to the locking position, and the power spring unit discussed later in the chapter. Lastly, the latch is rigidly attached to the pylon and connected to the body of the prosthetic knee using a four-bar linkage that creates the virtual locking axis of the prosthesis. At the transition point the linkages of the four-bar move the latch back, and therefore, unlocking the knee for flexion.

The full process of the engagement and disengagement of the latch mechanism can be divided into 4 phases for one full gait cycle:

Phase 1: At heel strike the latch is engaged, and the GRF at the foot causes a flexion moment about the knee. However, the tip of the latch is mechanically coupled with the knee piece and resists any flexion about the knee.

Phase 2: The GRF moves from the heel to the toes and causes an extension moment about the knee. The extension moment pushes the knee piece into the hard stop on the knee body, and therefore disengages the "hook" and the latch. Moreover, the GRF moves the latch backwards providing clearance for the knee piece to rotate about the knee axis.

Phase 3: As the knee is flexing during the late stance and swing flexion phases, the bias spring returns the latch back for the re-engagement of the knee piece and the latch.

Phase 4: During late swing extension, the lower leg of the prosthesis is swung forward, bringing the latch and the knee piece together. The knee piece pushes the latch against the bias-spring and relocks the knee right before heel strike.

In order to ensure the safety of the user, the structural integrity of the components were analyzed. According to able-bodied gait data, the design must withstand at least a flexion moment of 0.7 Nm/kg. The moments about the prosthetic knee joint were calculated using a free body diagram. During stance phase, the only force that could cause the latch structure to fail is the reaction force between the latch tip and the "hook" of the knee piece when the knee is subjected to a flexion moment. Therefore,

the safety factor of the latch can be calculated using beam bending theory and tensile strength calculations. Moreover, in order to increase the safety factor of the latch locking mechanism, the parts were machined out of Aluminum 7075, which has higher strength properties than Aluminum 6061 that was used for other parts of the knee. The resulting safety factor was 1.4, meaning that the mechanism can withstand a flexion moment of 1 Nm/kg during stance phase. All of the components of the latch mechanism were machined on a CNC mill, and Oilite bronze bushings were used for low friction force at the rotational components of the prototype.

Early Stance Flexion (ESF)

In able-bodied gait, knee flexion during stance phase provides shock absorption for the hip joint and results in approximately 15-20 degrees of knee flexion as the leg is loaded under the body's weight. Prostheses designed for the developing world generally do not include early stance flexion functionality, which results in a gait pattern visibly different from able-bodied gait and potential health problems in the future.

In the component optimization algorithm, the necessary torque for early stance phase knee flexion was best replicated with a spring K_{ESF} that created a moment T_{ESF} about the knee axis as the knee flexed θ (Eqn. 2.4). However, preliminary testing showed that the algorithm's predicted ideal stiffness value for this spring was uncomfortable for the users [19].Therefore, the early stance unit was designed with an adjustable stiffness in order to determine the optimal values experimentally.

$$T_{ESF} = -K_{ESF} * \theta \tag{2.4}$$

The current design affords an adjustable stiffness by employing a slot where a linear spring can be moved closer or further away from the flexion axis. Moreover, the spring has an adjustable preload in order to eliminate backlash in the device, which has been reported to be uncomfortable in the previous iterations of the design, and create a minimum torque that has to be applied to the knee before it can actually be flexed [19]. Therefore, the knee would not start to flex immediately after heel strike

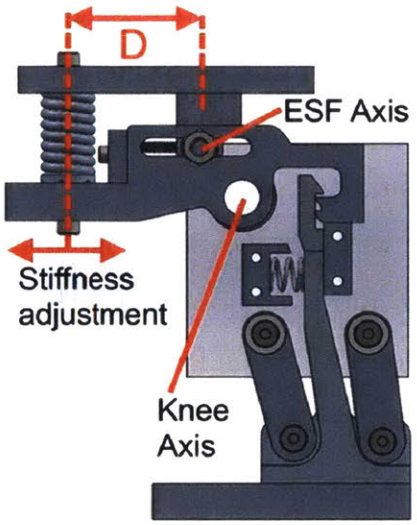

Figure 2-8: In the knee assembly cross section the early stance flexion module is attached to the knee part with a separate axis that can be tuned for the user. The stiffness can be adjusted with lateral movement of the spring (controlled by distance D) and the spring slot can be open on the ends for easier loading and unloading of springs.

and create a feeling of instability as if the knee is buckling, and will only start to flex when the knee is properly loaded by the user. Lastly, the flexion axis can also be adjusted in order to account for varying GRF profiles. The GRF profiles are likely to be different depending on the user of the prosthetic knee, as it is influenced by such factors as the prosthetic foot design, experience using a prosthesis, and the compensatory walking techniques.

The early stance flexion module allows a stiffness range of 0.8-7.0 Nm/kg-rad, compared to the optimal value of 0.87 Nm/kg/rad, and has to be adjusted for each user. The ESF unit is attached to the knee piece, which is in turn attached to the upper leg. Therefore, it can only be engaged during stance phase flexion, and doesn't affect the locking mechanism.

Power Spring Unit

The power spring unit serves two functions. During the transition between the stance and swing phases when the locking mechanism opens, it assists knee flexion. During late swing phase, it acts as a bumper to provide resistance to minimize the shock

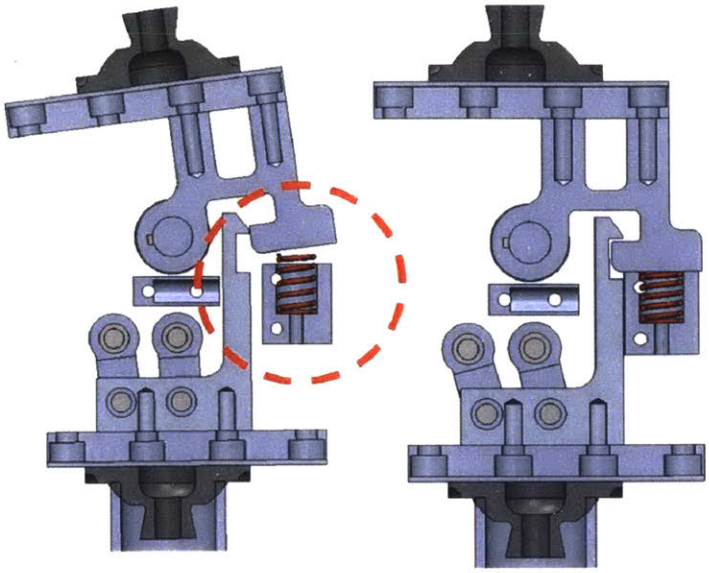

Figure 2-9: Power spring in the knee prototype assembly cross section. The power spring is a linear spring inside a hard stop attached to the knee body. It is compressed when the latch is locked.

as the latch locks. Therefore, the design of the power spring needs to include the optimal value of stiffness K_{PS} (Eqn. 2.5), and an optimal angle range θ_{PS} that the stiffness acts over.

$$T_{PS} = -K_{PS} * \theta \tag{2.5}$$

In the current prototype, the power spring unit was created with a linear spring that is installed on the knee body inside a hard stop that limits the knee piece extension motion. The value of the spring stiffness and angle range can be adjusted using spacers under the spring, and therefore change the amount of spring compression, or by switching out the spring for higher or lower stiffness. The spring is compressed between the hard stop and the knee piece as the latch is locked during swing extension. As the latch is unlocked, the stored energy in the spring is used to push the knee piece, which is now engaged with the damper, and assist flexion of the knee joint.

All components except for the damping module are discussed in detail in this chapter. The damping module concept is introduced in this section, however, since it is the main module of interest of this thesis, the detailed process of modeling,

designing, and manufacturing is presented in Chapter 3, and the characterization and in-vivo testing are presented in Chapter 4.

Damping Module

Although, the modeling, design, and testing of the damping module is presented in detail in the next chapter, it is important to note the main function that the damping unit plays with respect to the overall knee design. This section describes how the component selection was influenced by early prototypes of the knee prosthesis and the current main design focus.

In the ideal component selection estimated by Narang [34, 35], two constant-force dampers were required to replicate able-bodied gait: one damper during late stance and swing flexion and one friction damper during swing extension. It should be noted that the damper value for knee flexion is 4.2 times larger than the damper value for swing extension. Moreover, the dampers are only engaged for a part of the flexion or extension phases, which is hard to achieve without using separate clutches for each component.

The early prototypes that used optimal damping predicted by Narang [34] showed swing phase control; however, the constant-force dampers did not fit the high performance required [19], which is discussed in more detail in Section 3.1. In order to improve the replication of the target knee moment, viscous rotary dampers were selected, and the ideal damping moment was modeled with the following relation:

$$T_{damper} = -B_{damper} * \omega \tag{2.6}$$

This analysis has shown that the optimal component selection does not include damping during knee extension phase. This could be a result of the knee moment and knee angular velocity being "out-of-phase" with each other. Moreover, during testing of early design prototypes, users preferred no damping during knee extension, as that would allow the knee to extend and lock earlier during the gait cycle. The ability to visibly see that the foot was ready for heal strike gave a sense of security

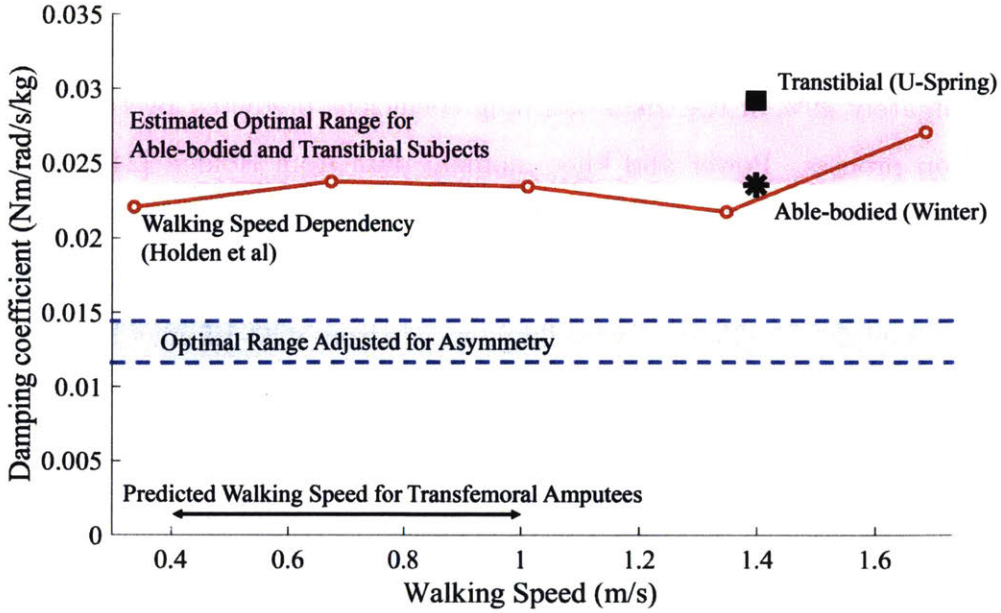

Figure 2-10: Optimal damping range of $B_{dampingrange} = 0.012 - 0.014 Nm/(kg*rad/s)$ displayed with a blue band with blue dashed outline was determined by estimating the damping range for able-bodied and transtibial subject displayed with pink band and scaling the damping to account for asymmetry during swing phase. Moreover, data from Holden [24] suggests that the damping coefficient would not change for walking speeds below 1.4 m/s. Transfemoral amputees are expected to walk with a walking speed range of 0.4-1.0 m/s.

that the knee would not buckle when leg is loaded. Therefore, the design presented in the next chapter was made specifically only for late stance and swing flexion of the knee.

The range of optimal damping was estimated from the optimal damping coefficient calculated from U-spring data and able-bodied data (Fig. 2-10). The upper limit is set by determining the optimal components for knee moment replication for a transtibial amputee ($B = 0.029\frac{Nm}{kg*\frac{rad}{s}}$)) with all leg segment masses set to 100%. The lower limit is set by an optimal damping coefficient from component optimization for an able-bodied subject ($B = 0.024\frac{Nm}{kg*\frac{rad}{s}}$)) from Winter [46].

Lastly, the optimal damping value had to be adjusted to account for slower walking speed and gait asymmetry common for transfemoral amputees. The asymmetry in transfemoral gait results in a shorter knee flexion phase during late stance and swing. Using empirical data from Jaegers [26] the able-bodied knee flexion is approximately

two times longer than transfemoral knee flexion for the same walking speed, which results in a twice larger knee angular speed. Therefore, the damping coefficient would be approximately 49% of the ideal damping coefficient predicted by the component optimization process. Power and knee moment data from Holden [24] was used to identify the effect of walking speed on the damping coefficient. Optimal damping coefficients were estimated for walking speeds form 0.33-1.68 m/s. The results have shown that damping coefficient for walking speeds from 0.33-1.5 m/s has only small changes ($\pm 10\%$), however for fast walking speeds (above 1.5m/s) the damping coefficient significantly increased. Since persons with transfemoral amputation tend to walk with slower walking speeds, we concluded that the walking speed will likely not affect the optimal damping coefficient. More details on the effects of walking speed and asymmetry on the damping scaling process is presented in the PhD thesis of Arelekatti [].

Therefore, $B_{damping\,range} = 0.012 - 0.014 \frac{Nm}{kg * \frac{rad}{s}}$ was identified as the range of optimal damping coefficients for a transfemoral amputee to best replicate the target knee moment, and therefore, achieve able-bodied kinematics during swing phase. The range takes into account the effect of the prosthetic foot by using data for a person with a transtibial amputation to set the upper limit of optimal damping coefficients. Moreover, the optimal damping range estimation accounts for characteristic gait deviation for a person with a transfemoral amputation.

Chapter 3

Damper Design

The main focus of this study was exploring the role of damping in a single-axis prosthetic knee by designing a damper to achieve able-bodied kinematics. The main functional requirements for the damper prototype are presented below:

- The design of the prototype should be simply integrated into the knee prototype (radius up to 1.75") and should be easily and quickly interchanged during testing with a transfemoral amputee.

- The design of the prototype should be minimally adjusted in order to provide a range of damping values for comparison of gait kinematics.

- The design has to be characterized and the performance has to be validated in lab before testing with a transfemoral amputee.

The framework of component selection and optimal value estimation was presented in the previous chapter. This chapter will present an overview of the role of damping in prosthetic knees, examples of prior art, the design modeling, two explored rotary damper designs, and a detailed description of an experimental setup for damper characterization.

3.1 Damping role, existing dampers, and previously used dampers

As described in Section 2.2, Narang [34, 35] has proposed using dampers as a way to generate negative work during terminal stance and swing and, therefore, control the knee flexion during those phases. Specifically, the damping in prosthetic knees will be used as a deceleration device during knee flexion as a person transitions between stance and swing phases. For example, in the case of no damping, peak knee flexion angle can be larger than the required knee flexion for toe clearance and could actually delay the gait cycle duration and return of the foot for the next heel strike. On the other hand, if the damping torque at the knee joint is too large, the knee flexion would not be sufficient for ground clearance and would require the user to employ compensating strategies for ground clearance that were described in the Introduction. Such behavior can result in a higher metabolic cost of walking [27] and, most importantly, asymmetric gait would be visibly different from able-bodied kinematics, which is one of the main requirements for this project.

Damping control is commonly used in knee prosthesis designs in mature markets. For example, many designs have used fluid-based systems (pneumatic and hydraulic), that are either controlled passively or with a programmable, microprocessor actuator [22, 21, 29]. Generally, fluid-based solutions are expensive, bulky, and require periodic maintenance to prevent oil-leaks. In developing countries, due to pricing constraints, the prosthetic knees might not have any damping control, such as the two available options at BMVSS, or employ passive friction brakes that apply constant resistance [21].

The work by Narang [34] proposed the use of friction dampers to generate the moment about the knee. Initial designs of the prosthetic knee employed the friction brakes and demonstrated results that were consistent with the theoretical findings. Although this solution was cost-effective and simple, it also provided many performance challenges. First of all, the friction torque changed depending on the wear and the environmental conditions such as humidity and dust [19]. Moreover, the constant-

force friction dampers exhibited stick-slip behavior, which made the prosthetic knee prototype uncomfortable to use and resulted in an intermittent and inconsistent gait [19] However, the biggest limitation of constant friction dampers was unresponsive to changes in cadence, because even if the damper is installed and tuned correctly by a prosthetist, it will only be satisfactory for a small range of walking speeds [29]. For example, if an amputee decides to walk with a slower walking speed, the damper will cause toe-dragging. On the other hand, if the amputee decides to walk with a faster walking speed, the friction damper would not provide enough control over the heel rise. In both cases, the gait of the amputee would become visibly asymmetric and would not resemble able-bodied gait.

Fluid-controlled dampers, on other hand, are cadence-dependent and allow a smooth and consistent motion throughout the gait. For the prosthetic knee design two damping designs were identified as plausible solutions: linear fluid-based damper and rotary fluid-based dampers [[19]]. The theoretical performance of all three solutions (friction, linear hydraulic, and rotary hydraulic) were evaluated using the method described in Section 2.2, and the results identified that both hydraulic solutions provide a more accurate replication of the target knee moment [19]. Although, hydraulic linear dampers are the most common choice for knee flexion control, the solution wasn't effective for the current single-axis knee design and the user requirements. Specifically, linear dampers tend to have a more complex and expensive design due to a required hydraulic accumulator and tight tolerances to prevent leakage from the sliding seal. Additionally, the damping torque for linear dampers is proportional to the square of the linear velocity of the piston, which can be unintuitive and uncomfortable to the amputees. Rotary hydraulic dampers, on the other hand, are simple to integrate into the current single-axis knee design and, because of a rotating sealing, have a lower chance of leakage. Moreover, the damping torque for the rotary dampers is linearly proportional to the angular velocity about the knee axis. Lastly, the design can be very compact if a high viscosity fluid is used. Commercial rotary damper options were tested as a potential solution, specifically ACE dampers FDT-57 and FDT-63 [7], however, these dampers provided linear damping only up to 1 rad/s and could

not be easily modified to achieve the optimal value for a subject.

Therefore, in order to improve the functionality of the prosthetic knee and have control over the knee flexion during late stance and swing flexion, a custom rotary hydraulic damper design had to be built.

3.2 Modeling of Dampers

As described previously in Section 2.2, the component value selection was based on a knee moment as a target and kinematics about the knee joint as the input. The value for the components was selected based on the highest RMS value. Due to the architecture of the knee prosthesis, specifically the latch system, the engagement of the damping unit starts at the maximum extension of the knee before the terminal stance and ends at the maximum flexion of the knee during swing (Fig. 3-1). The ideal rotary damping coefficient (B_{damper}) was calculated using the equation below:

$$T_{damper} = -B_{damper} * \omega \tag{3.1}$$

where T_{damper} is the generated knee moment and ω is the reference knee angular velocity.

The optimization process estimated an ideal normalized by body weight damping coefficient that was adjusted in order to account for gait asymmetry common for transtibial amputees. More details on damping coefficient estimation are presented in the previous chapter.

3.3 Damper Designs

After the rotary fluid-based damper was selected for damping control during late stance and swing flexion, different hydraulic rotary damper designs were explored. This section presents two main damper prototypes: concentric fins and stacked disk designs. The fin design was used as a proof-of-concept that performed well, however, did not meet the size requirements; specifically, the build height of the dampers was

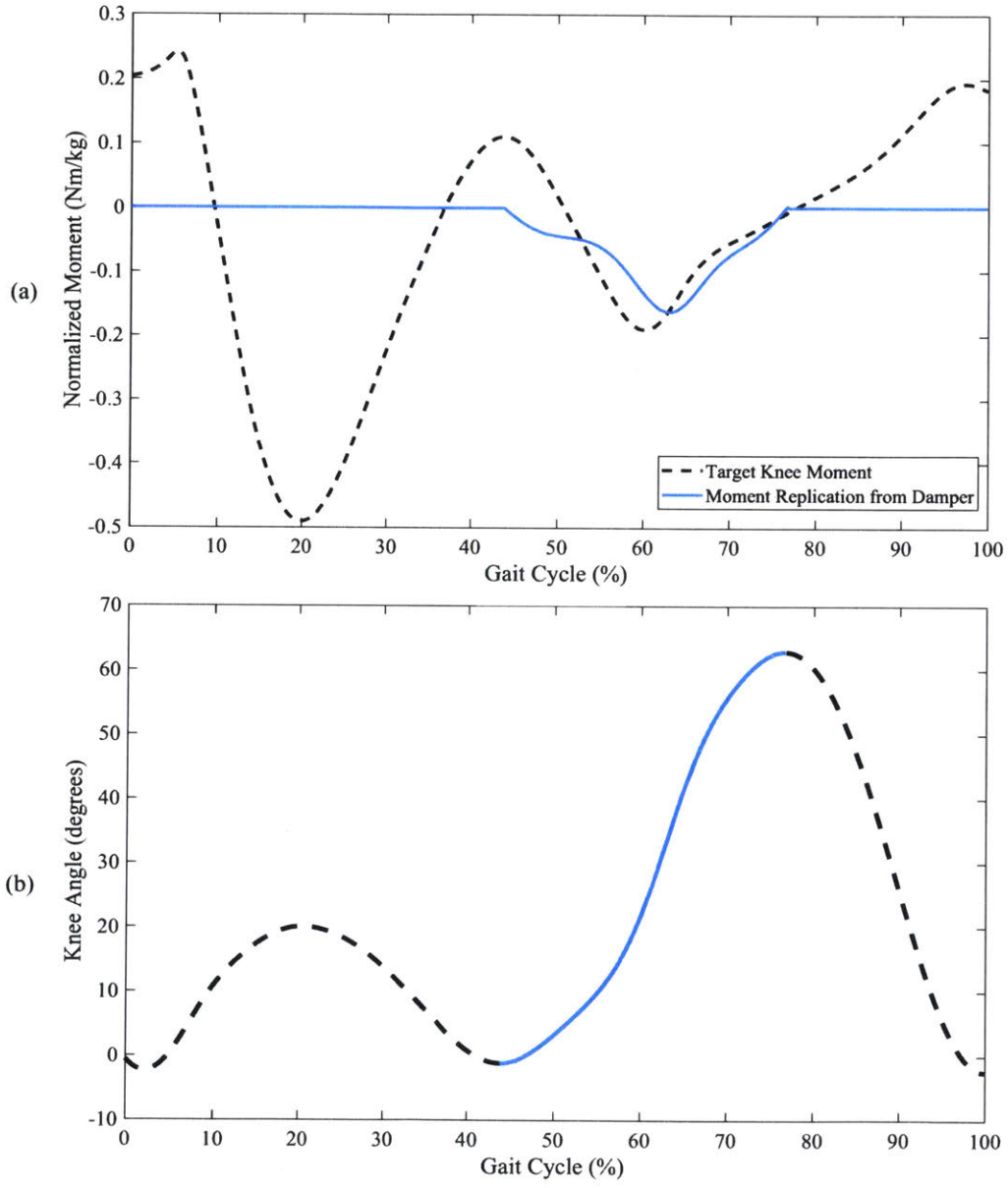

Figure 3-1: (a) An example of knee moment replication with only the damper and locking mechanism active. The computed value was adjusted after to account for gait asymmetry common for persons with a transfemoral amputation. (b) Zone of the gait cycle when the damper is activated.

too large. The stacked disk design allowed to damper height reduction and required range of damping.

3.3.1 Meshed Concentric Fin Design

The fin design described in this chapter was based on the rotary damper prototype that was built as a concept exploration for the prosthetic knee [19]. In the study, the damper prototype used shearing forces between two concentric walls, and the gap in between the walls was filled with highly viscous fluid. Although the prototype displayed the proper damping behavior, the measured damping was lower than the predicted optimal damping.

This study explored an updated fin design that included stator and rotor parts with multiple fins. The fins of the stator parts mesh concentrically about the knee axis with rotor fins, while leaving a small gap between the walls of the fins (Fig. 4-2). The stator fins were rigidly connected to the housing of the damper, which in turn is rigidly coupled to the body of the knee prosthesis. The rotor part was rigidly coupled with the knee axis shaft through a clutch, which allowed to quickly and easily remove and switch between dampers during testing of the prosthesis. As the latch unlocked and the knee started to flex, the rotor part of the damper starts to rotate respectively to the stator part of the damper.

The space between the fins is filled with highly viscous fluid. For this architecture the relationship between the angular velocity of the knee joint and the created damping moment can be derived by calculating the viscous shear stress at the stator wall and integrating the stress along the fin walls:

$$B_{fin} = \frac{2\pi\mu l}{t} R_1^3, \tag{3.2}$$

where B_{fin} is the resulting damping coefficient for one fin, R is the radius of the exterior surface of the stator wall, l is the height of the fin wall, t is the gap thickness between neighboring fins, w is the thickness of the fin wall, μ is the dynamic viscosity of the fluid in the gap. All of the presented variables are also shown in a detailed

schematic (Fig. 3-2).

The total damping torque for n rotator fins is presented in the following relationship:

$$B_{total} = \sum_{i=1}^{n} \frac{2\pi\mu l}{t}((R_1 - (n-1)D)^3 + (R_1 - w - (n-1)D)^3,) \quad and\, D = 2(w+t), \tag{3.3}$$

where D is the distance between the between two consecutive sets of interacting fins.

The viscous fluid that was sheared between the fins is a highly viscous silicone oil (Polydimethylsiloxane) and has a dynamic viscosity of 100 Pa-s [2]. For example, water and honey have a dynamic viscosity of 100mPa-s and 10 Pa-s, respectively. The high viscosity of the silicone fluid allowed us to make the dampers compact, while still being safe for human use [2] and easily accessible due to popular use in cosmetics and industry. However, the fluid also exhibited a shear-thinning behavior, when the viscosity of the fluid decreases as the velocity gradient in the fluid increases. This phenomenon was taken into account during the modeling of the damping using rheological data provided by the manufacturer [9].

The fins for the prototype were 3D printed using ABS plastic (Fig. 3-2). The knee axis shaft of the prosthetic knee was coupled with the rotor part through a one way needle roller clutch. The use of a one way clutch allowed the application of damping torque during the terminal stance and swing knee flexion, by having the knee shaft locked in one direction of rotation (knee flexion), and free rotation in the other direction (knee extension). One-way roller needle clutch [6] with a maximum torque rating of 23.05 Nm was chosen in order to have a safety factor of 1.5 based on the measured maximum knee moment in able-bodied studies [46]. All of the described parts were fitted into a housing that was CNC machined out of acetal resin. In order to seal the fluid inside the damper during the rotation, and constrain the motion of the rotor along the knee axis, an acetal resin housing cap manufactured using a laser cutter and a CNC mill with a rotary shaft seal [4] were used between the stationary and rotary parts. An additional O-ring was used in order to prevent fluid leakage between the housing cap and the housing.

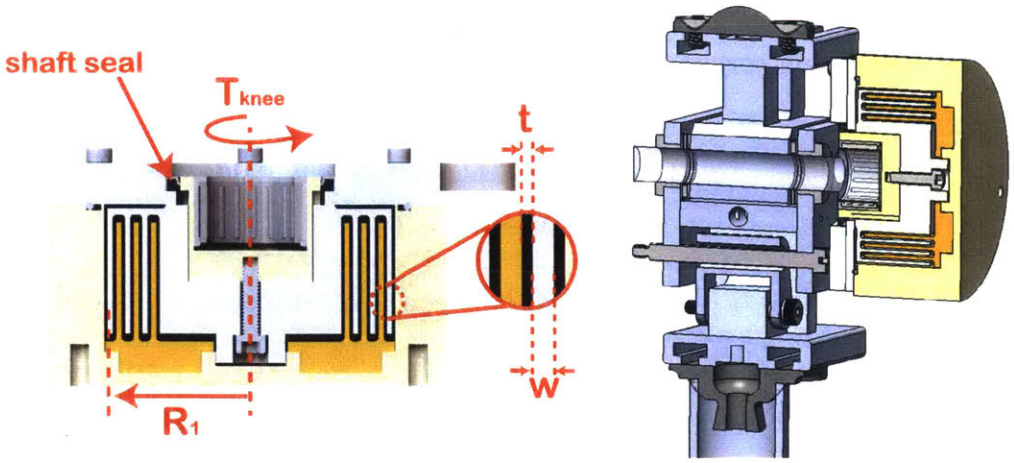

Figure 3-2: Schematic of a cross-section of a damper with concentric fin walls that shear silicone fluid in the gap between neighboring walls. (a) Characteristic dimensions required for calculating damping coefficient and the damping moment T_{knee} are the maximum radius R_1, wall thickness w, and gap thickness t. A shaft seal prevents silicone oil leakage. (b) Cross section of the knee prototype assembly shows that the damper is coupled to the knee axis with a one-way clutch.

In order to validate the optimal range of damping values, three dampers with the fin architecture were built: low, optimal, and high dampers. The optimal damping was chosen for a person with a body mass of 75 kg. The low, optimal, and high dampers corresponded to two, three, four fins respectively, and resulted in damping coefficients of 0.8 Nm/rad/s, 1.5 Nm/rad/s, and 2.2 Nm/rad/s.

Although the design allowed us to achieve optimal damping and performed well in testing with an above-knee amputee, which is described in Section 4.2, the height

Number of walls	3
Maximum wall radius (inches)	1.25
Wall Height (inches)	1
Gap Thickness (inches)	0.025
Wall Thickness (inches)	0.050
Overall Damper Height(inches)	2
Damper Weight(grams)	400

Table 3.1: Characteristic dimensions for a meshed fin damper prototype with 3 fin walls required for the damping coefficient calculation and overall build height and weight of a damper.

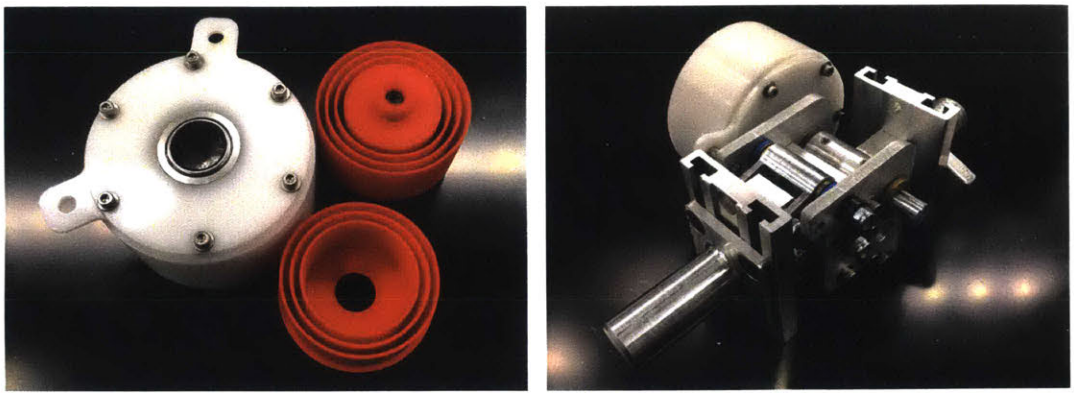

(a) (b)

Figure 3-3: (a) Photograph of a fin architecture damper and the 3D printed rotor and stator parts that concentrically mesh between each other. (b) Photograph of the damper in the knee prototype assembly.

had to be reduced in order to be not noticeable in trousers. In order to decrease the height of the damper, multiple strategies have been investigated based on the governing equation (Eqn. 3.3). As the damping coefficient is proportional to the cube of the radius, increasing the radii of the fin walls would be the most effective solution. However, the exterior radius could not be increased as it would become too large for the knee prototype and would not satisfy the size requirement. Moreover, the fin wall closest to the exterior radius has the greatest contribution to the overall damping coefficient. Therefore, adding fins closer to the axis of rotation would not significantly increase the damping coefficient. Using fluid with greater dynamic viscosity or decreasing the gap thickness were not sufficient solutions due to the shear thinning effects described previously. Therefore, in order to meet the size requirements, a new design had to be used for the testing of the prosthetic knee.

3.3.2 Stacked Disk Architecture

In order to meet the size requirements, and specifically, a lower build height, a different design was explored. The new design employed a stacked disk architecture instead of the concentric fin wall design described in the subsection above. This design allowed us to achieve ideal damping coefficients, while keeping the exterior radius the same and decreasing the build height by up to 50%.

$$B_{disk} = \frac{\pi \mu R}{t} \tag{3.4}$$

$$B_{disk} = \frac{\pi (R_1^4 - R_2^4)}{t} \int_{R_2}^{R_1} \mu dR \tag{3.5}$$

Such an improvement was possible due to the increase of the viscous fluid shearing area [45]. The resulting relationship between the damping torque at a radius between a stationary and rotary disk is proportional to the radius to power of four (Eqn. 3.4), unlike the fin design, where the damping torque is proportional to the cube of the radius. This change allowed us to decrease the build height of the dampers. Similar, to the concentric fin design, the model of the damper accounted for the shear-thinning phenomena, by calculating the velocity gradient at different radii from the inner to the outer radii of the disks (Eqn. 3.5). In the new design the stationary disks are coupled to the housing using a set of four tabs on the exterior radius of the disk. The rotary disks are coupled to the clutch coupler using a set of tabs on the interior radius of the disk. The clutch is then coupled to the knee axis shaft of the prosthetic knee. The space between the disks was filled with the same high viscousity fluid as described in the previous design, and the gap thickness was controlled using thin rings. A detailed schematic of the interior of the damper for the disk assembly is presented in Fig. 3-4.

One of the advantages of the stacked disk design was the flexibility of damping coefficient adjustment, because the damping coefficient could be controlled by the number of rotary disks (Eqn. 3.6). For example, a damper of size n would have n rotor disks and $n-1$ stator disks. The total build height of the damper would also depend on the number of disks, disk thickness (t_{disk}), gap thickness(t_{gap}), and the build height from cap (t_{cap}) and housing($t_{housing}$) (Eqn. 3.7).

$$B_{total} = n * B_{disk} = n * \frac{\pi (R_1^4 - R_2^4)}{t} \int_{R_2}^{R_1} \mu dR \tag{3.6}$$

$$H_{damper}^{n} = (2n-1)t_{disk} + 2nt_{gap} + t_{cap} + t_{housing} \tag{3.7}$$

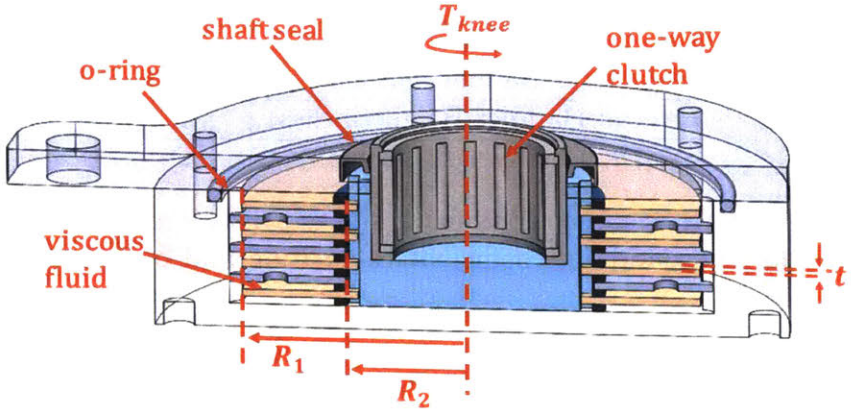

Figure 3-4: Schematic of a cross-section of a damper with stacked disks that shear silicone fluid in the gap between disks. Characteristic dimensions required for calculating the damping coefficient are the outer radius (R_1), inner radius (R_2), and gap thickness (t). A shaft seal[4] prevents silicone oil leakage and the one-way clutch [6] allows for damper activation only during knee flexion.

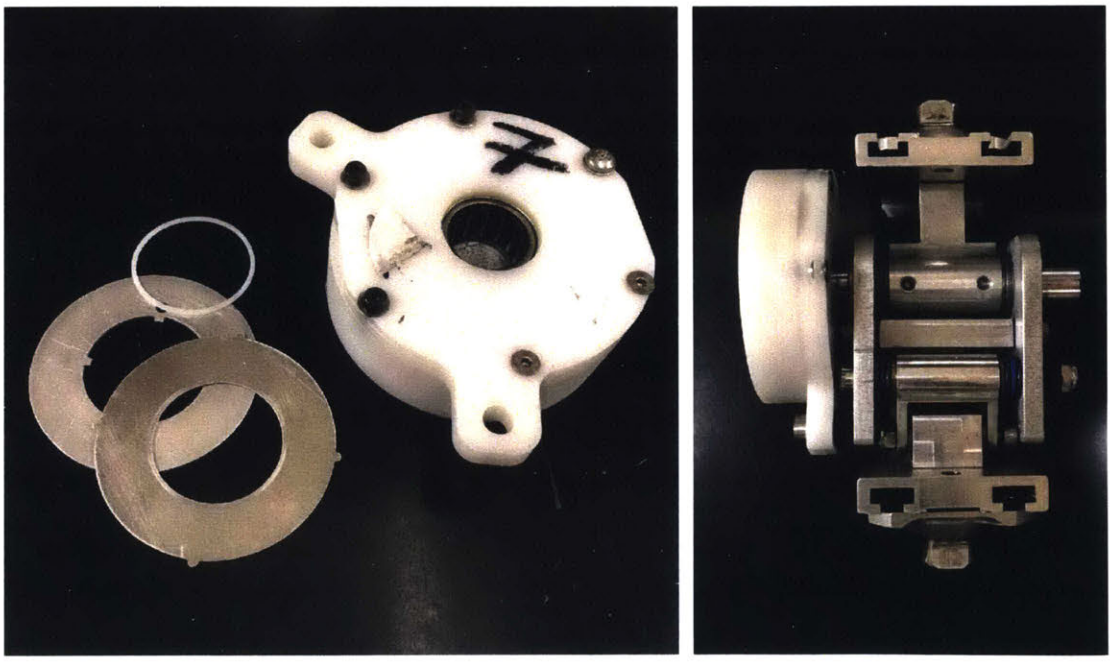

Figure 3-5: (a) Photograph of a stacked disks architecture damper, the rotor and stator disks, and the disk spacer that controls the gap thickness. (b) Photograph of the damper in the knee prototype assembly.

Number of disks	5
Gap Thickness (inches)	0.03125
Disk Thickness (inches)	0.025
Inner Radius (inches)	0.69
Outer Radius (inches)	1.18
Overall Damper Height(inches)	1
Damper Weight(grams)	220

Table 3.2: Characteristic dimensions for a stacked disks damper prototype with 5 disks required for the damping coefficient calculation and overall build height and weight of a damper.

The housing, the housing cap, the shaft seal, one-way roller clutch, and the O-ring designs were repeated from the fin architecture. The stator and the rotor disks were manufactured from an aluminum sheet using an abrasive waterjet machine. The aluminum sheet thickness and the width of the disk tabs were chosen to prevent failure of the tabs from shearing. The coupler between the clutch and the disks was manufactured out of aluminum using a CNC mill and lathe. Lastly, the disk spacers were laser cut out of acetal delrin sheet. As an example, all dimensions for a damper with five rotary fins are presented in Table 3.2.

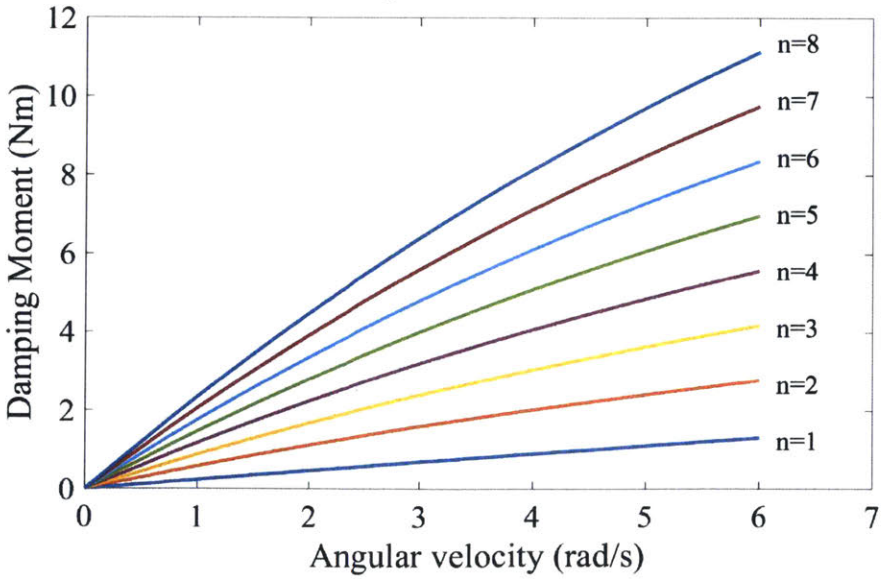

Figure 3-6: The damping moment versus the angular velocity model for the stacked disk architecture for 1 through 8 disks.

Overall, 8 different dampers were built with the number of rotary disks ranging

Number of disks	$A(Nm/(rad/s)) * x$	$B(Nm/(rad/s)) * x + C(Nm)$
1	0.21x	0.20x+0.04
2	0.45x	0.40x+0.21
3	0.67x	0.60x+0.30
4	0.90x	0.80x+0.41
5	1.11x	1.00x+0.51
6	1.33x	1.20x+0.60
7	1.55x	1.39x+0.73
8	1.79x	1.59x+0.84

Table 3.3: Best fit coefficients to the model of dampers. A is the coefficient, assuming there is no damping torque at zero velocity. B and C coefficients are coefficients for a linear fit.

from 1 to 8 disks. This range of damping coefficients allowed us to accommodate variable body masses, inertial properties of leg segments, walking speeds, and gait asymmetry. For all of the damping cases, the best fit coefficients are presented in Table 3.2 and the resulting model of damping moment versus angular velocity is presented in Fig. 3-6.

3.4 Experimental Validation

A custom mechanical testing setup was built in order to validate and characterize the damper prototype before testing the damper with a transfemoral amputee. A velocity-controlled DC motor (Vex Robotics MINI CIM [11]) spun the rotor part of the damper at a set speed. A magnetic encoder was used to control the speed of the motor and sent the velocity measurement to be collected by the controller. The housing and, thus, the stator part of the damper was rigidly connected through a lever arm of a set length to a load cell (Omega Engineering LC101-250 [8]), which measured the moment experienced by the damper. The load cell readings were amplified with a load cell amplifier (Tacuna Systems [10]) and collected by the controller. In order to account for machining errors, a flexible shaft coupling with an angular and parallel misalignment capability of up 1.5 degrees and 0.028 inches, respectively, was chosen. The experimental setup was controlled using a Visual Basic platform supported by VexRobotics.

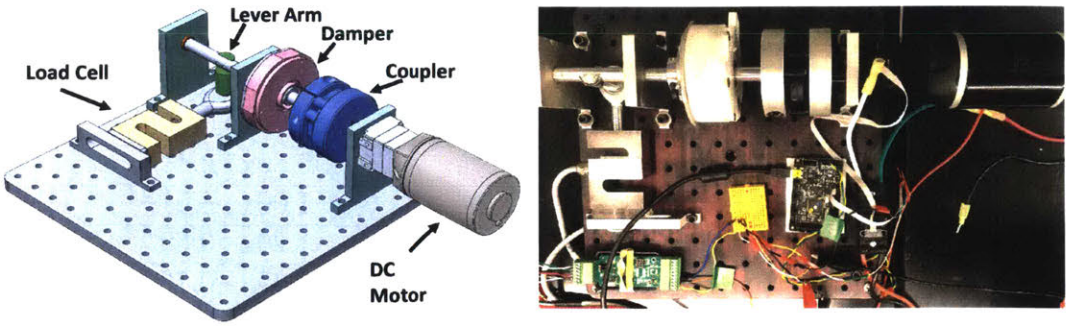

Figure 3-7: The solid model (a) and photograph (b) of the damper characterization setup. The rotor part of the damper is spun by a DC motor, the stator part of a damper is connected to a load cell using a lever arm to measure the torque experienced by the damper.

A detailed schematic and an image of the setup is presented below:

The load cell measurements were tuned with calibration weights and the full experimental setup was validated with the commercial fluid-based rotary dampers mentioned in Section 3.1, the ACE dampers FDT-57 and FDT-63 [7]. The damping moment as a function of rotation velocity measured by the experimental setup matched the data sheet values for both of the dampers with a percent deviation of up to 6%.

Chapter 4

Testing, Results, and Discussion

This chapter presents the results from experimental studies conducted in order to validate the damper design and optimal range selection presented in the previous chapters:

- Damper design characterization using an experimental setup in lab validated that a wide range of damping coefficients is available for in-vivo testing

- Feedback and pilot data from preliminary qualitative testing in India with BMVSS patients confirmed that the gait kinematics and user perception are sensitive to the choice of damping coefficient

- Quantitative kinematic study with subjects walking on a treadmill with the prosthesis confirmed that increased damping decreases peak knee flexion angle and damping is required to prevent hyperflexion

- Quantitative kinematic and kinetic study of normal over-ground walking with the prosthesis confirmed that the optimal damping range predicts a damping coefficient such that peak knee flexion angle is close to able-bodied

For each of the studies, this chapter also discusses the contributions and limitations.

4.1 Damper Characterization

The testing protocol for each of the disk dampers consisted of a damping moment measurements at six different speeds (from 1 rad/s to 6 rad/s). The angular velocity limit of 6 rad/s was based on the maximum angular velocity at the knee joint measured for an able-bodied gait [46]. For each of the velocities the damper experienced ten full rotations at a constant speed and the average damping moment was calculated. In the mechanical setup described in Section 3.4, the angular velocity was measured using a magnetic encoder and the damping moment was calculated from the reaction force measurement from the load cell. The dataset was then processed and analyzed through custom scripts implemented in MATLAB (The MathWorks, Inc, Natick, MA).

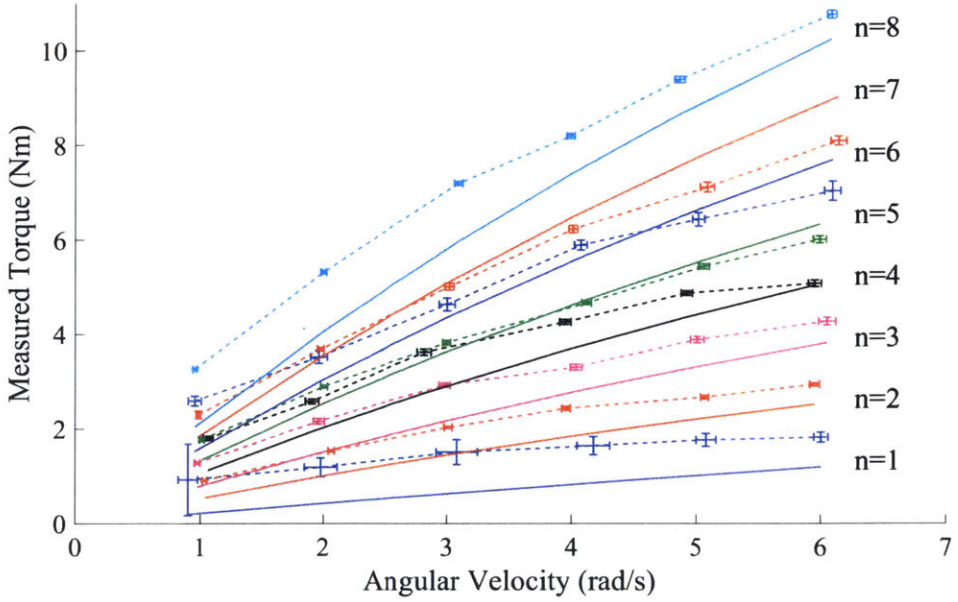

Figure 4-1: Experimental data from stacked disks damping characterization for the number of disks ranging from 1 to 8 disks. The solid line represents the model for the damper and the dashed line represents the data from testing at six different speeds with the standard deviation.

The resulting characterization plots of damping torque for the stacked fin architecture versus angular velocity are presented in Fig. 4-1 and best-fit coefficients for linear fit are presented in Table 4.1. All of the dampers exhibited a non-linear profile,

with the damping torque increasing as the number of rotary disks increases. Overall, for dampers with 4 through 8 disks, the data matched the model well (within 10%) at higher angular velocities and showed a higher difference at lower speeds (about 30%). Moreover, for dampers 4 through 8, the linear coefficient without y-intercept matched the model coefficient within 0.1 Nm/rad/s. For dampers with 1 to 3 rotary disks, the model did not match the data. However, the calculation of the damping coefficients shown in Table 3.3 suggests that this result is caused by mechanical friction between the clutch coupler and the housing cap, as the linear slope coefficient is within 0.02Nm/rad/s. Unlike dampers 4 through 8, the clutch coupler in dampers 1 through 3 extended past the housing cap which could result in additional friction in the dampers.

In order to determine the cause of the error between the data and the model, multiple error sources were evaluated: filling dampers, sensitivity of the gap thickness, and viscosity changes from temperature. The filling of dampers was evaluated by measuring the weight change before and after the damper was filled, and confirming that the dampers were fully filled with silicone oil. Moreover, vacuum chambers were used in order to ensure that the silicone oil did not absorb air and trap bubbles, and thus, decrease the damping coefficient. The sensitivity of the gap thickness analysis has shown that a 10% gap error would result in approximately up to 8% difference in the damping coefficient. Using data from the silicone oil datasheets, it was determined that a temperature increase of 1 degree Celsius would result in approximately 1% decrease in damping torque. Moreover, during the experiments, a thermal camera recorded that the clutch coupler experienced a temperature change of up to 5 degrees Celsius for dampers with five or more disks. Lastly, the datasheet for the silicone oil stated that there could be an up to 10% error in viscosity parameters, which would result in approximately up to 7% difference in the damping coefficient. Therefore, the difference between the data and the model can be explained by the three error sources evaluated above.

Overall, the simple viscous friction model for damper design was found to be an extremely useful tool to size the damper prototype before empirical characterization

Number of disks	$A(Nm/(rad/s))x$	$B(Nm/(rad/s))x + C(Nm)$
1	0.37x	0.18x+0.85
2	0.56x	0.40x+0.68
3	0.80x	0.58x+0.96
4	1.10x	0.68x+1.35
5	1.10x	0.84x+1.13
6	1.32x	0.90x+1.87
7	1.44x	1.12x+1.46
8	1.80x	1.44x+2.06

Table 4.1: Best fit coefficients for different damping conditions calculated from damper characterization experiments. The coefficient A presents the damping coefficient assuming the y-intercept coefficient is 0, and B is the linear coefficient with a non-zero y-intercept coefficient C, which accounts for mechanical friction in the system.

through mechanical testing. Although a more accurate theoretical model would be required for mass manufacturing of the damper, the results show that the dampers present a range of 0.37-1.80Nm/rad/s damping coefficients, which covers the required range for optimal damping testing.

4.2 Preliminary Results from Qualitative Study at BMVSS

After the mechanical testing and characterization, the damper with concentric fin architecture along with the current prosthetic knee prototype were brought for qualitative testing with an above-knee amputee at BMVSS in Jaipur, India. The MIT Committee on the Use of Humans as Experimental Subjects approved the protocol for this study. The subject that participated in the study had a unilateral amputation, and used a manual locking single-axis prosthetic knee, provided by BMVSS. The relevant human parameters presented in Table 4.2 were used to calculate the corresponding low, optimal, and high damping coefficients. Before testing, the prosthetic knee was fitted by a trained prosthetist, and the subject was asked to walk for 10 minutes in order to get used to the knee, specifically, the locking mechanism.

The goal of this study was to validate the performance of the damper and the

prosthetic knee by collecting qualitative feedback from the subject and observing the change in the gait depending on the different damping conditions. The experiments would determine if the optimal value predicted by the model allows a comfortable swing control, and compare the performance of the optimal damper to a damper with lower and higher resistance. Overall, four damping conditions were tested in the study: no damping, low, optimal, and high damping. Along with the prosthetic knee described in Section 2.3 and the dampers, the experiment used the Jaipur Foot, a standard pylon, and a standard socket available at the BMVSS.

For each of the damping conditions, the subject was asked to walk for approximately 10 minutes per damping condition. The dampers were tested in the order of increasing damping coefficient, however, the damping condition was not revealed to the subject in order to assess if the subject is capable of detecting differences between the conditions. Each trial was video-recorded with an iPhone 6 camera, and after the trial was over qualitative feedback form the subject and the prosthetist was collected. The recorded video was tracked using MATLAB and image tracking DLTdv digitizing tool [23].

The experiments showed that the subject could easily distinguish between each condition. Moreover, there was visible difference in gait for each of the four conditions tested. First of all, the subject reported a small difference between the no and low damping conditions, and would prefer more resistance from the damper. The high damping case, on the other hand, prevented comfortable toe clearance, and was the only case when the subject required more effort and actually needed to concentrate in order to smoothly transition between swing and stance. Lastly, the subject reported that optimal damping case was the most comfortable for him, as it allowed the smoothest transition between gait cycle phases and required the least conscious

Gender	Male
Height (cm)	175
Weight (kg)	75

Table 4.2: Body parameters of the participant from preliminary qualitative study at BMVSS.

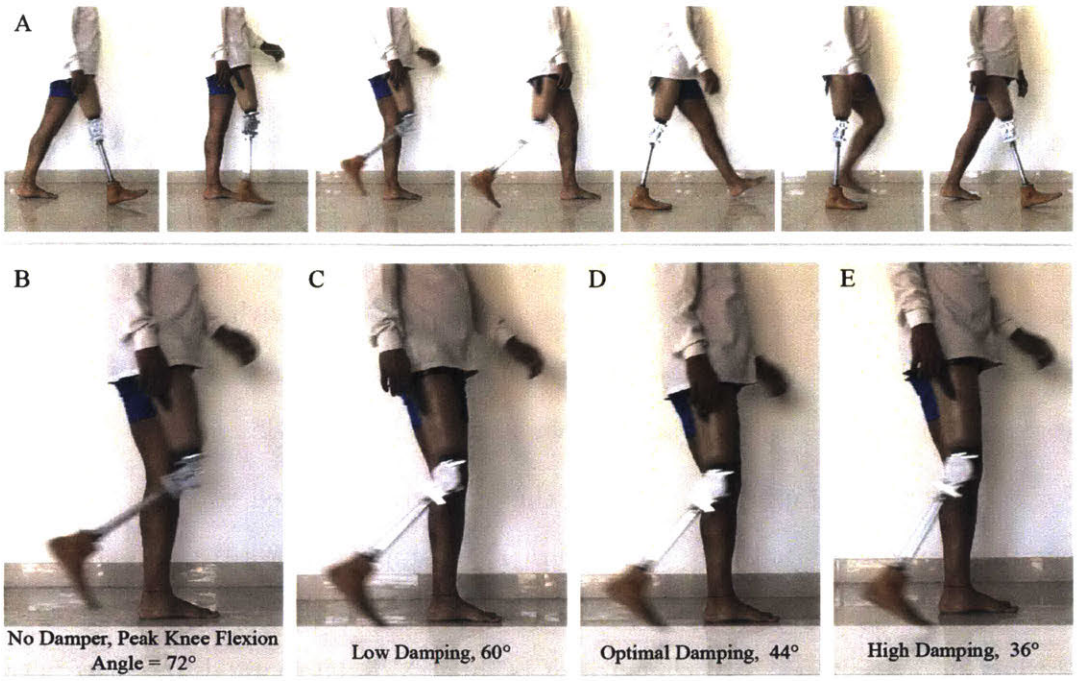

Figure 4-2: Results from the preliminary qualitative study in India showed that different damping conditions could visually change the gait. A. The subject walking comfortably after acclimatization, snapshots through a full gait cycle are shown (read left to right). There is no damping module attached. B-E. The approximate values of peak flexion angle through the swing phase were calculated using the image processing toolbox on MATLAB [23].

effort when walking. Therefore, the testing confirmed that the model allowed us to predict a value that is in the correct range of an optimal value. However, a full kinematic and kinetic study is required for more accurate information in order to validate that the peak knee flexion angle decreases as the damping coefficient increases and how each damping condition affects the knee moment.

4.3 Treadmill testing

4.3.1 Testing Protocol

The goal of this study was to quantify how the damping coefficient affects the gait kinematics of a person with a transfemoral amputation walking at a given speed. Moreover, this study was used as preparation for a motion capture study described in

the next section, as it provided subjects with acclimatization and practice time and allowed the prosthetist to reduce the time required for fitting during motion capture trials by taking notes on alignment. The study was conducted at the Northwestern University Prosthetics-Orthotics Center (NUPOC), and the experimental protocol was approved by both MIT Committee on the Use of Humans as Experimental Subjects (COUHES) and the Institutional Review Board (IRB) at Northwestern University (NU).

Before testing, the prosthetic knee was fitted by a trained prosthetist, and the subject was asked to walk for 5-10 minutes in order to get used to the knee, specifically, the locking mechanism. During the acclimatization period, the subject would walk with no damper and one of the dampers in order to get used to both setups. The prosthetic foot used for this experiment was the U-spring foot described in Section 2.1; and the springs and the beam on the foot were chosen depending on the weight of the participant. The prosthetic knee described in Section 2 was used with only the locking and damping modules, in order to concentrate only on the performance of the damper. A standard pylon was used to connect the knee and foot, and the subject used their own socket and suspension.

In the beginning of the experiment the subject was asked to walk with a no damper condition and a comfortable walking speed on the treadmill was established. Keeping the walking speed the same, the dampers were tested in order of increasing damping, and for each of the damping conditions data were collected for at least 20 steps on the treadmill. After each damping condition, the subject was asked to provide qualitative feedback through a survey and the participants could rest as needed between conditions. Kinematic data were collected using inertial measurement units (IMUs) that were installed on the prosthetic side. The dataset was then processed and analyzed through custom scripts implemented in MATLAB (The MathWorks, Inc, Natick, MA).

Overall, seven subjects participated in the treadmill testing; all of the subjects had a unilateral above-knee amputation. Average age, height, weight, and years since amputation are presented in the Table 4.3.

Number of participants	5 (2 male, 3 female)
Average age (years)	54±10
Average years since amputation (years)	27±19
Average height (cm)	171±7
Average weight (kg)	79±10

Table 4.3: Average body parameters from subjects in the treadmill study. All subjects satisfied the inclusion criteria defined by the COUHES and IRB at NU.

4.3.2 Treadmill Study Results and Limitations

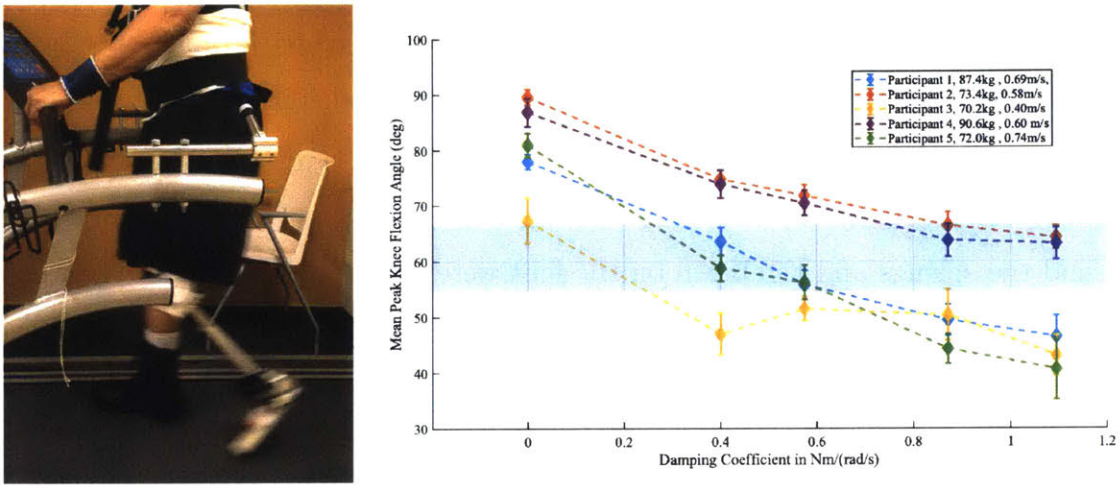

Figure 4-3: Treadmill study has shown that mean peak knee flexion angle decreased as the damping coefficient increased. The subjects walked at a constant speed on a treadmill with different damping conditions. All subjects were able to achieve knee flexion in the able-bodied range (gray band shows one standard deviation for able-bodied subjects). The no-damping condition resulted in hyperflexion during swing phase for all of the subjects. The error bars show the standard deviation of the measurements.

The experiments showed that at constant walking speed an increase in the damping coefficient resulted in a decrease in peak knee flexion angle during swing. However, the flexion angle would increase when the participant employed a compensation behavior (circumduction and hip-hiking) during swing. For all of the subjects, the no-damping case resulted in hyperflexion of the knee joint, suggesting that a damper is required to achieve an able-bodied gait. It is also important to note that the subjects preferred walking speeds (0.4-0.75m/s) that were much lower than the walking speed of the subject for the target data set from the U-spring study (1.4m/s). Lastly, the

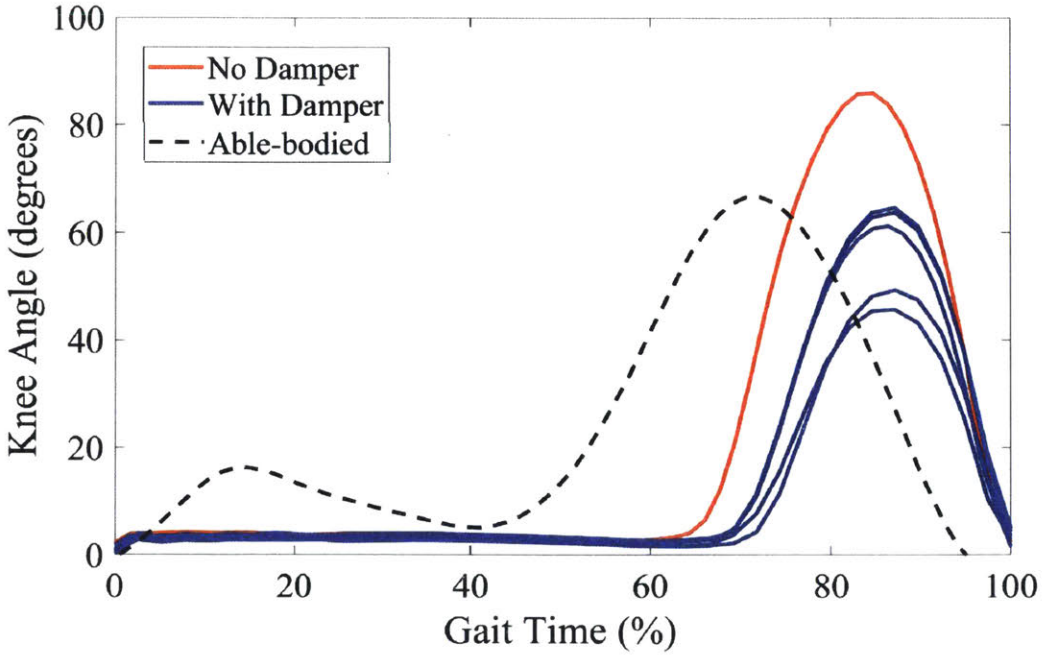

Figure 4-4: The treadmill study confirmed the asymmetry hypothesis and swing flexion phase length for transfemoral amputees was shorter by 33% and 50% for no-damping and damping cases respectively compared to able-bodied data from Winter [46]

experiments also confirmed the asymmetry of gait, with swing flexion starting later in the gait cycle (Fig. 4-4). Compared to able-bodied kinematics, in the no-damping case, the swing flexion phase was 33% shorter, and for the other damping case, the knee flexion was 50% shorter that the swing flexion for able-bodied subject [46].

This study was conducted using a treadmill in order to keep the walking speed constant. However, the gait on the treadmill can be significantly different from over flat ground walking [28]. Therefore, the optimal damping coefficient for walking on the treadmill may be different for over-ground walking. Therefore, a full kinematic and kinetic quantitative experiment on flat ground is required to validate the model for optimal damping for everyday use of the prosthetic knee.

4.4 Motion Capture Experiment

4.4.1 Testing Protocol

The reliability, comfort, and approximate physical behavior of the prototype were established through mechanical testing of the dampers on the benchtop experimental setup, preliminary qualitative study at BMVSS, and quantitative kinematic study on the treadmill. In order to validate the optimal damping coefficient range and test the sensitivity of gait to different damping conditions, a quantitative gait analysis study was conducted with Dr. Matthew J. Major, Jenny A. Kent, and Rebecca Stine at the Motion Analysis Research Laboratory at the Northwestern University (NU). The component optimization model as well as damping scaling presented in Section 2, were validated by collecting kinematic and kinetic data and comparing the measured optimal damping that resulted in appropriate peak knee flexion to the modeled optimal damping range.

The study at the Motion Laboratory was performed according to approved protocols from the MIT Committee on the Use of Humans as Experimental Subjects (COUHES) and the Institutional Review Board at Northwestern University. Three unilateral above-knee prosthesis users (2 females, 1 male) between the age of 18 and 65 years old were recruited by our collaborators at NU. The average age, height, and weight are presented in Table 4.4.

After the informed consent of the selected subject, retro-reflective markers were attached bilaterally by the study team to the participant's anatomical landmarks (Fig. 4-5). Subjects were asked to walk on flat ground using the knee prototype in order to acclimate to the prosthesis. Similarly to the treadmill experiments, the prosthetic leg consisted of the U-spring foot set for the weight of the subject, prosthetic knee

Subject	1	2	3
Gender	Male	Female	Female
Height (cm)	178	166	152
Weight (kg)	84.3	68.7	54.9

Table 4.4: Body parameters of the subjects from the Motion Capture study.

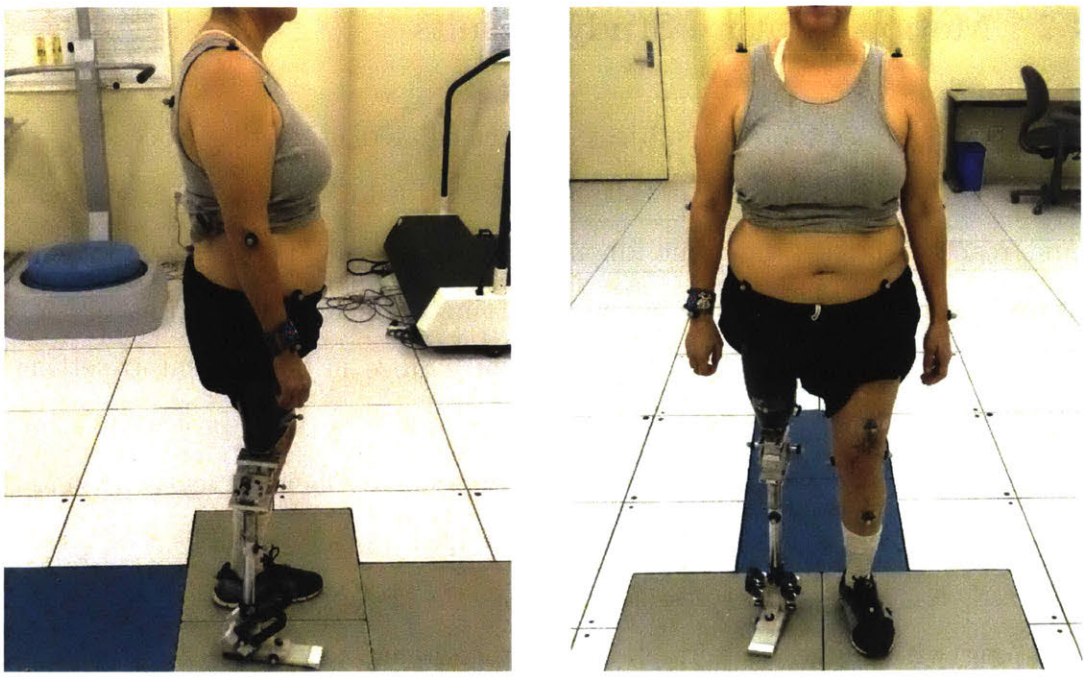

Figure 4-5: Gait lab setup and marker positions on the transfemoral subject standing on the force plates and testing the prosthetic leg prototype in the no-damping condition.

without the early stance flexion and power spring modules, standard pylon, and subject's socket and suspension.

Each subject was asked to test 5 damping conditions: no-damping condition and four dampers around the optimal damping range calculated for the subject. Similar to previous studies, the damping conditions were tested in increasing order of damping. The subjects were then asked to walk at a comfortable speed on the walkway until the gait kinematic and kinetic data were collected for at least five steps for each of the damping conditions. Between each condition the participants could rest as needed and no realignment of the prosthesis was required, as each component of the prosthetic leg was firmly attached to one another. The kinematic data were collected through a motion capture system that tracked the reflective markers, and the kinetic data were measured using force plates embedded in the walkway. Several pictures and videos were taken during each trial using equipment in the Motion Laboratory. The entire set of data was then processed and analyzed through custom scripts implemented in Matlab (The MathWorks, Inc, Natick, MA).

4.4.2 Motion Capture Study Results

The joint kinematics for each subject were calculated using the process of inverse dynamics with inertial parameter estimation described in Section 2.1 from measured ground reaction forces and joint kinematics. Using calculated knee moment and measured knee angular velocity, a true damping coefficient was estimated for each subject and then normalized by body weight. Since in the benchtop setting the dampers were evaluated in isolation from the prosthetic knee prototype, the true damping coefficients were different from the damping coefficient measured in Section 4.1 due to off-plane loads and friction in the knee prototype. The measured true normalized damping coefficients showed that the dampers provided a wide range of damping with higher, lower, and similar damping coefficients to the predicted optimal range (Fig. 4-6 (a)). Therefore, according to the true damping coefficient measurement, the conditions closest to the optimal range for subjects were: Condition c for Subject 1, Condition d for Subject 2, and Condition d for subject 3.

Similar, to the treadmill study the mean peak knee flexion angle on the prosthetic side decreased as the damping coefficient increased (Fig. 4-6 (b)). Each subject was able to achieve a knee flexion within one standard deviation of the target knee flexion of 64 degrees. Condition A with the lowest damping coefficient resulted in hyperflexion for each subject, suggesting that dampers are required to achieve able-bodied kinematics during flat-ground walking. The damping condition that provided the knee angle closest to the target knee angle was in the optimal range of $0.012 - 0.014 \frac{Nm}{kg * \frac{rad}{s}}$ only for Subject 2, for other two subjects a lower damping coefficient resulted in the target knee flexion. However, for all of the subjects the true damping coefficients closest to the optimal damping range allowed to achieve the target peak knee flexion within one standard deviation. Therefore, the damping condition within the optimal range for damping would have resulted in the target knee flexion angle.

However, for all of the subjects the peak knee flexion angles on the sound side for each condition was within the second standard deviation from the able-bodied target. This suggests that the target knee angle might be lower than the estimated

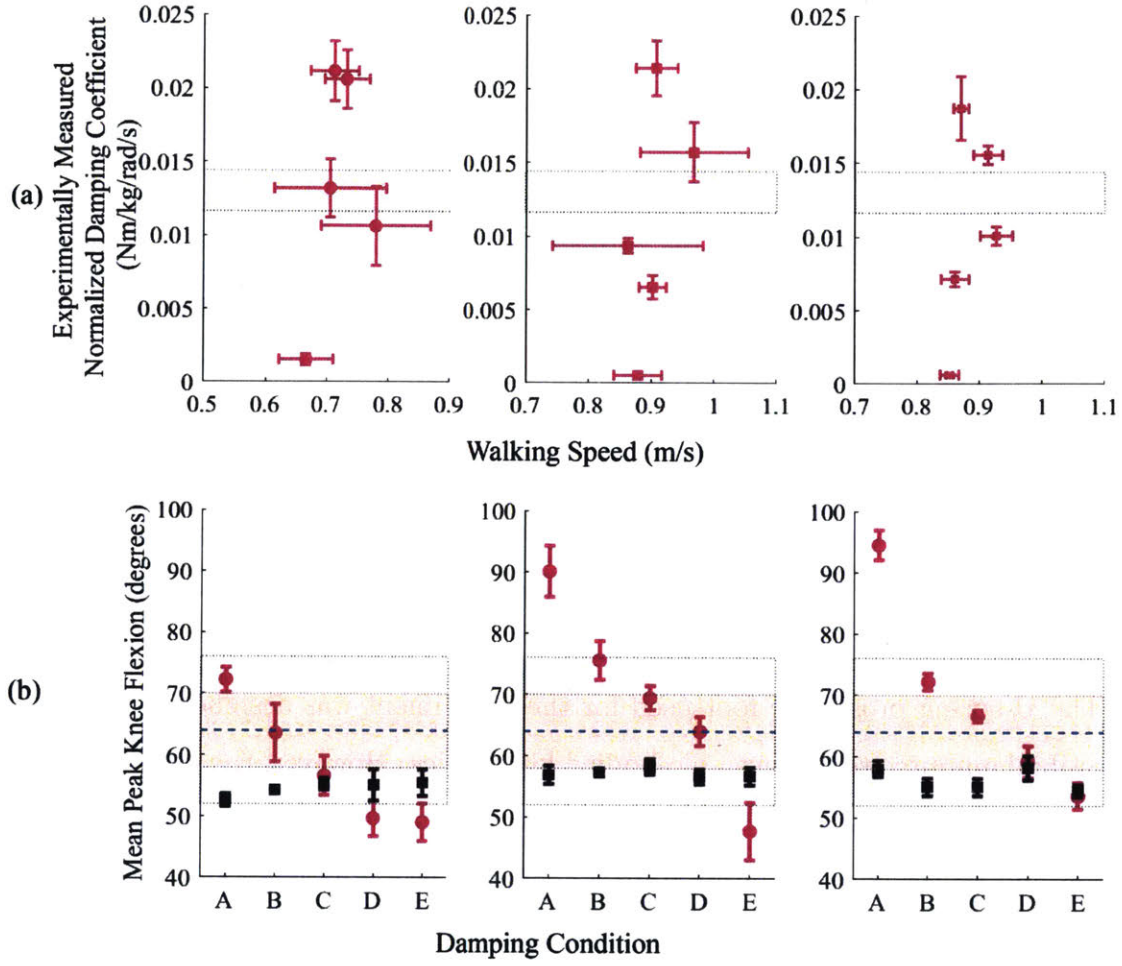

Figure 4-6: Results from the motion capture study for three subjects. (a) Experimentally measured normalized damping coefficients with respect to the optimal damping range shown with a gray band. Dampers provided a wide range of damping coefficients with two conditions close to the predicted optimal values of damping. (b) Measured mean peak knee flexion angle for prosthetic side (purple) decreased with increasing damping coefficient for all subjects, while the knee angle on the sound side (black) remained the same and lower than target for each damping condition. The dashed line shows the reference able-bodied peak knee flexion [46]. For all of the graphs the error bars show the standard deviation of the measurements.

reference target. This could be a result of slower walking speeds (0.7-0.9m/s) than the reference able-bodied walking speed (1.4 m/s). Moreover, comparing the knee angle on the prosthetic side with the sound side, the damping condition that allowed closest replication of sound side matched with the conditions closest to the optimal damping range.

4.4.3 Study Limitations

This study was conducted on three subjects who were asked to walk at self-selected speeds on flat ground. Although the average walking speed changed between conditions for each subject by up to 0.1 m/s, the independence of optimal damping range selection from walking speed was not confirmed. The study has to be repeated for a larger set of subjects and in different walking speed scenarios before any generalization can be made about the effect of walking speed on optimal damping. Additionally, the target peak knee flexion needs to be investigated in order to account for slower walking speeds.

The U-spring prosthetic foot used for the experiment was designed in order for a transtibial amputee to achieve able-bodied kinematics. However, the gait and loading of the foot may be different for a transfemoral amputee. Moreover, the early stance flexion and power spring module were not used in the experiments in order to evaluate the performance of damping independently. Therefore, the performance of the prosthetic foot could be influenced by the lack of knee flexion during stance.

Lastly, another limitation of this study is the inertial parameters approximation described in Section 2.1. The coefficients available in the literature give an average approximation depending on the body mass and may not be correct for every person. Additionally, many amputees experience muscle atrophy on the side of amputation, which results in lower mass of the residual limb. Since the muscle mass would be different for each subject, this factor was not included in the estimation of the leg segment inertial parameters.

Chapter 5

Conclusions

This study presents a physical design of a damper prototype for a passive single-axis prosthetic knee in order to validate the optimal damping range for achieving able-bodied kinematics. Able-bodied kinematics were defined as one of the main functional requirements for a prosthetic knee for users in developing countries, specifically in India. The modeling and testing of prosthetic knee design presented in this thesis were done in collaboration with V.N. Murthy Arelekatti.

The optimal damping range for a rotary fluid-based damper was determined by selecting passive components to best replicate a target knee moment for an able-bodied subject and transtibial amputee wearing a fully characterized prosthetic foot. The component optimization determined that damping is required during late stance and swing flexion in order to decelerate the leg and prevent hyperflexion. The target knee moment was adjusted for changes in inertial parameters, and the damping range was scaled to 49% to account for gait asymmetry common for persons with a transfemoral amputation. The resulting optimal range for damping coefficients normalized by body mass was estimated as $0.012 - 0.014 \frac{Nm}{kg * \frac{rad}{s}}$.

Eight dampers were built with a range of damping coefficients from 0.37 to 1.80 Nm/(rad/s) providing a wide range of damping coefficients to be tested with transfemoral amputees. The damper have a stacked fin architecture, where a highly viscous fluid is sheared between neighboring disks. The resulting design was easy to integrate into the modular design of the prosthetic knee and could be quickly interchanged

during clinical studies.

After dampers were characterized on an experimental setup in lab, preliminary qualitative testing was conducted in Jaipur, India, with a subject with a unilateral transfemoral amputation. The study has shown that the prosthetic knee with the damper allowed a smooth transition between stance and swing, maintained structural integrity, was received well by the subject, and the damping range allowed to visibly change the gait. A quantitative kinematic study with five transfemoral amputees walking on a treadmill showed that increasing the damping coefficient decreases the peak knee flexion angle and confirmed the gait asymmetry hypothesis. Lastly, a quantitative study in a gait lab was conducted with three subjects with a transfemoral amputation to measure the kinetic and kinematic performance of the prosthetic knee. The true damping coefficient was estimated using the measured moment and angular velocity about the knee joint. The damping conditions close to the optimal damping range showed a peak knee flexion angle close to the target knee angle. Therefore, the optimal damping range for late stance and swing flexion allows the peak knee flexion angle achieved to be close to able-bodied.

Future Work

Future work for this study should focus on confirming that the optimal damping coefficient does not change depending on the walking speed, and therefore one damper can be used for different cadences. More testing has to be done with the early stance flexion and power spring modules, in order to optimize the kinematics throughout the entire gait cycle, especially when the power spring is interacting with the damper.

Moreover, using the frameworks for the prosthetic foot and knee, a prosthetic leg could be designed and optimized. For example, a prosthetic foot could be designed for the above-knee amputees to account for differences between transfemoral and transtibial amputation by minimizing the error in the hip location.

Additional work should also be done in order to improve the functionality of the prosthetic knee and include other gait activities such as walking at different speeds, on slopes or uneven terrains. Lastly, the final design of the prosthetic knee and

the dampers has to be fatigue tested before mass-manufacturing and distribution at BMVSS in India.

Bibliography

[1] Bhagwan Mahaveer Viklang Sahayata Samiti: What we do. http://jaipurfoot.org/what_we_do/.

[2] Clean, Clear, Silicone Oils and Lubricants from Clearco. http://www.clearcoproducts.com/ (Accessed 08/2019).

[3] D-Rev. Remotion: A high-performance knee joint for amputees everywhere. http://d-rev.org/projects/mobility/.

[4] Grease Seal for 1-1/8" Diameter Shaft, 1.375" OD. https://www.mcmaster.com/5154t61.

[5] Man-Systems Integration Standards. https://msis.jsc.nasa.gov/sections/section03.htm.

[6] One-Way Locking Needle-Roller Bearing Clutch. https://www.mcmaster.com/2489k6.

[7] Rotary dampers - motion control-products-ace controls inc. https://www.acecontrols.com/ (Accessed 08/2019).

[8] S-Beam Load Cell. https://www.omega.com/en-us/sensors-and-sensing-equipment/load-and-force/load-cells/lc101/p/LC101-200.

[9] Silicone Fluid: stable, inert media. https://www.gelest.com/wp-content/uploads/Goods-PDF-brochures-inert_silicones_2013.pdf.

[10] Strain Gauge or Load Cell Amplifier/Conditioner Interface. https://tacunasystems.com/products/amplifiers-conditioners/strain-gauge-or-load-cell-amplifier-conditioner-interface-2/.

[11] VEX Robotics Mini CIM Motor. https://www.vexrobotics.com/217-3371.html.

[12] *Observational gait analysis.* Los Amigos Research and Education Institute, Inc. Rancho Los Amigos National Rehabilitation Center, 4th edition, 2001.

[13] J. Andrysek. Lower-limb prosthetic technologies in the developing world : A review of literature from 1994 - 2010. *Prosthetics and Orthotics International*, 34(December):378–398, 2010.

[14] Jan Andrysek, Susan Klejman, Ricardo Torres-Moreno, Winfried Heim, Bryan Steinnagel, and Shane Glasford. Mobility function of a prosthetic knee joint with an automatic stance phase lock. *Prosthetics and Orthotics International*, 35(2):163–170, 2011.

[15] V N Murthy Arelekatti, Nina T Petelina, W Brett Johnson, Amos G Winter V, and Matthew J Major. Design of a Passive, Shear-Based Rotary Hydraulic Damper for Single-Axis Prosthetic Knees. In *Proceedings of the ASME 2018 International Design Engineering Technical Conferences and Computers and Information in Engineering Conference. Volume 5A: 42nd Mechanisms and Robotics Conference. Quebec City, Quebec, Canada. August 26âĂŞ29, 2018.*, nov 2018.

[16] Venkata Narayana Murthy Arelekatti. *Design of fully passive prosthetic knee for persons with transfemoral amputation in India.* Number 2010. Master's Thesis. Massachusetts Institute of Technology. Cambridge, MA, 2015.

[17] Venkata Narayana Murthy Arelekatti. *Frameworks for the design of passive prosthetic knee components using user-centered methods and biomechanics of level-ground walking.* PhD thesis, Massachusetts Institute of Technology, 2019.

[18] Anamika Arya, Adrian Lees, H C Nirula, and Leslie Klenerman. A biomechanical comparison of the SACH, Seattle and Jaipur feet using ground reaction forces. *Prosthetics and orthotics international*, 19 1:37–45, 1995.

[19] Molly A Berringer, Paige J Boehmcke, Jason Z Fischman, Athena Y Huang, Youngjun Joh, J Cali Warner, V N Murthy Arelekatti, Matthew J Major, and Amos G Winter. Modular Design of a Passive, Low-Cost Prosthetic Knee Mechanism to Enable Able-Bodied Kinematics for Users With Transfemoral Amputation. In *ASME 2017 International Design Engineering Technical Conferences and Computers and Information in Engineering Conference*, pages V05BT08A028—-V05BT08A028. American Society of Mechanical Engineers, 2017.

[20] Paolo De Leva. Adjustments to zatsiorsky-seluyanov's segment inertia parameters. *Journal of Biomechanics*, 29(9):1223–1230, 1996.

[21] Alex Furse, William Cleghorn, and Jan Andrysek. Development of a low-technology prosthetic swing-phase mechanism. *Journal of Medical and Biological Engineering*, 31(2):145–150, 2011.

[22] Steven A Gard. The Influence of Prosthetic Knee Joints on Gait. *Handbook of Human Motion*, pages 1–24, 2016.

[23] Tyson L Hedrick. Software techniques for two- and three-dimensional kinematic measurements of biological and biomimetic systems. *Bioinspiration & Biomimetics*, 3(3):34001, 2008.

[24] John P Holden, Gloria Chou, and Steven J Stanhope. Changes in knee joint function over a wide range of walking speeds. *Clinical Biomechanics*, 12(6):375–382, 1997.

[25] Olga Horgan and Malcolm MacLachlan. Psychosocial adjustment to lower-limb amputation: a review. *Disability and rehabilitation*, 26(14-15):837–850, 2004.

[26] Sonja M.H.J. Jaegers, J. Hans Arendzen, and Henry J. de Jongh. Prosthetic gait of unilateral transfemoral amputees: A kinematic study. *Archives of Physical Medicine and Rehabilitation*, 76(8):736–743, 1995.

[27] Arthur D Kuo and J Maxwell Donelan. Dynamic principles of gait and their clinical implications. *Physical therapy*, 90(2):157–174, feb 2010.

[28] Song Joo Lee and Joseph Hidler. Biomechanics of overground vs . treadmill walking in healthy individuals. *Journal of Applied Physiology*, 104(3):747–755, 2008.

[29] Earl A Lewis. Fluid-Controlled Knee Mechanisms Clinical Considerations. *Bulletin of Prosthetics Research*, pages 24–56, 1965.

[30] Dinesh Mohan. A report on amputees in India. *Orthotics and Prosthetics*, 40(1):16–32, 1986.

[31] V N Murthy Arelekatti and Amos G Winter , V. Design and Preliminary Field Validation of a Fully Passive Prosthetic Knee Mechanism for Users With Transfemoral Amputation in India. *Journal of Mechanisms and Robotics*, 10(3), apr 2018.

[32] I C Narang and V S Jape. Retrospective study of 14,400 civilian disabled (new) treated over 25 years at an Artificial Limb Centre. *Prosthetics and Orthotics International*, 6(1):10–16, 1982.

[33] Yashraj S Narang, V N Murthy Arelekatti, and Amos G Winter. The effects of prosthesis inertial properties on prosthetic knee Moment and hip energetics required to achieve able-bodied kinematics. *IEEE Transactions on Neural Systems and Rehabilitation Engineering*, 24(7):754–763, 2016.

[34] Yashraj S Narang, V N Murthy Arelekatti, and Amos G Winter. The effects of the inertial properties of above-knee prostheses on optimal stiffness, damping, and engagement parameters of passive prosthetic knees. *Journal of biomechanical engineering*, 138(12):121002, 2016.

[35] Yashraj Shyam Narang and Others. *Identification of design requirements for a high-performance, low-cost, passive prosthetic knee through user analysis and dynamic simulation.* PhD thesis, Massachusetts Institute of Technology, 2013.

[36] Government of India National Sample Survey Organization, Ministry of Statistics and Programme implementation, India National Sample Survey Organisation, and Government of India National Sample Survey Organization, Ministry of Statistics and Programme implementation. Disabled persons in India National Sample Survey, 58th round, July - December 2002. *A. N. D. India*, 485(485):43 – 46, 2003.

[37] K M Olesnavage and A G Winter. A Novel Framework for Quantitatively Connecting the Mechanical Design of Passive Prosthetic Feet to Lower Leg Trajectory. *IEEE Transactions on Neural Systems and Rehabilitation Engineering*, 26(8):1544–1555, 2018.

[38] Kathryn M Olesnavage. *Development and validation of a novel framework for designing and optimizing passive prosthetic feet using lower leg trajectory.* PhD thesis, Massachusetts Institute of Technology, 2018.

[39] Jacquelin Perry and Judith M. Burnfield. Gait Analysis: Normal and Pathological Function., jun 2010.

[40] Victor Prost, Kathryn M Olesnavage, W Brett Johnson, Matthew J Major, and Amos G Winter V. Design and Testing of a Prosthetic Foot With Interchangeable Custom Springs for Evaluating Lower Leg Trajectory Error, an Optimization Metric for Prosthetic Feet. *Journal of Mechanisms and Robotics*, 10(2), mar 2018.

[41] C. W. Radcliffe. Four-bar linkage prosthetic knee mechanisms: kinematics, alignment and prescription criteria. *Prosthetics and Orthotics International*, (18):159–173, 1994.

[42] Jessica Rose and James G. Gamble. *Human Walking.* Lippincott Williams & Wilkins, 3rd edition, 2006.

[43] Bruce Rybarczyk, David L Nyenhuis, John J Nicholas, Susan M Cash, and James Kaiser. Body image, perceived social stigma, and the prediction of psychosocial adjustment to leg amputation. *Rehabilitation Psychology*, 40(2):95, 1995.

[44] Victor Prost. *Experimental Validation of the Lower Leg Trajectory Error, an Optimization Metric for Prosthetic Feet.* Master's Thesis. Massachusetts Institute of Technology. Cambridge, MA, 2017.

[45] Frank M. White. *Fluid Mechanics.* McGraw-Hill, 8th edition, 2016.

[46] David A. Winter. *Biomechanics and Motor Control of Human Movement.* John Wiley & Sons, Inc, 4th edition, 2009.

[47] Dominik Wyss. Evaluation and Design of a Globally Applicable Rear-locking Prosthetic Knee Mechanism. 2012.

[48] W. Yinusa and M. E. Ugbeye. Problems of amputation surgery in a developing country. *International Orthopaedics*, 27(2):121–124, 2003.